Reply to referee #2, Raphaela Vogel

Dear Raphaela,

We are grateful to you for the positive assessment of our study, for insightful remarks and for the valuable recommendations. We appreciate all the comments; we took them into account while preparing the revised version of the manuscript.

Below, the original comments are given in blue color.
The text added to the revised version of the manuscript is marked by red color.

> General comments:
> 1. Distinction of parameterization influence and resolution influence:
> At the end of Section 2.2.2, I was missing a discussion of the influence of the changing resolution between the PARAM and EXPL experiments. Only on p.13, L6 you mention that "differences between PARAM and EXPL in Fig. 4 illustrate the sensitivity of the response to horizontal resolution and the use of convective parameterization", but everywhere else you neglect the potential influence of the changing resolution on the results. Marsham et al. 2013 isolated the influence of the convective parameterization by comparing experiments with 12kmPARAM, 12kmEXP and 4kmEXP. I'd suggest you refer to their study noting that the most important differences between the experiments are due to the convective parameterization, and that the increasing resolution between the experiments with explicit convection merely leads to quantitative differences. It's of course a bit trickier than that, but I think you wouldn't need to go in much more detail.

This is a helpful suggestion. We were aware of this study, and the fact, that the differences found in this study were mainly quantitative for varying horizontal resolutions. The same became apparent for ICON in a small test case, which was not included in the paper. Therefore, we did not study it in more detail, but should have mentioned this in the article. We added the following sentences at the end of section 2.2.2:

> The same study differentiated between the effect of parametrization and the effect of horizontal resolution by comparing experiments with 12 km grid-spacing and both parametrized and explicit convection as well as explicit convection at 4 km. It was found that the dominating factor is the convective parametrization, which substantially alters the dynamics of the monsoon system, while the influence of the horizontal grid-spacing is mainly of quantitative nature. Building on these results, we will concentrate on differences between parametrized and explicit convection and pay less attention to resolution effects.

> 2. Negative & positive cloud feedbacks:
> On p. 19, L6&L34 I stumbled over the sentences referring to the negative and positive low-cloud feedbacks. The way it is written, one thinks that you actually enforced a reduction in low cloud, rather than just a change in their opacity. By making the low clouds less opaque, you just manipulate their radiative effect, but e.g. not their effect on the moisture budget or the microphysics. This should be made clearer.

We tried to explain this better by adding the following lines:

This denotes a negative feedback mechanism, as a (here enforced) reduction of low cloud opacity leads to more cloud production, at least in the early part of the day. Recall that the modification was only applied to the cloud optical thickness, as seen by the radiation scheme.

---

3. Influence of organization of convection:
I would like to see some more discussion about the influence of changes in the organization of convection on the results. From Marsham et al. 2013 I take that mesoscale convective systems and the associated storm outflows are a significant component of the WAM system and I assume that they will also affect differences between your PARAM and EXPL simulations. On p.31, L5 you mention that you find effects of convective organization in your simulations. I understand that a detailed analysis of the role of convective organization would be beyond the scope of the manuscript, but maybe you can already appreciate some of the differences by looking at profiles of moisture variance and their diurnal cycle (similar to Figure 7). This might also be important for radiatively-driven secondary circulations that likely contribute to organizing the convection. I'd be surprised if changes in convective organization wouldn't be important in your experiments.

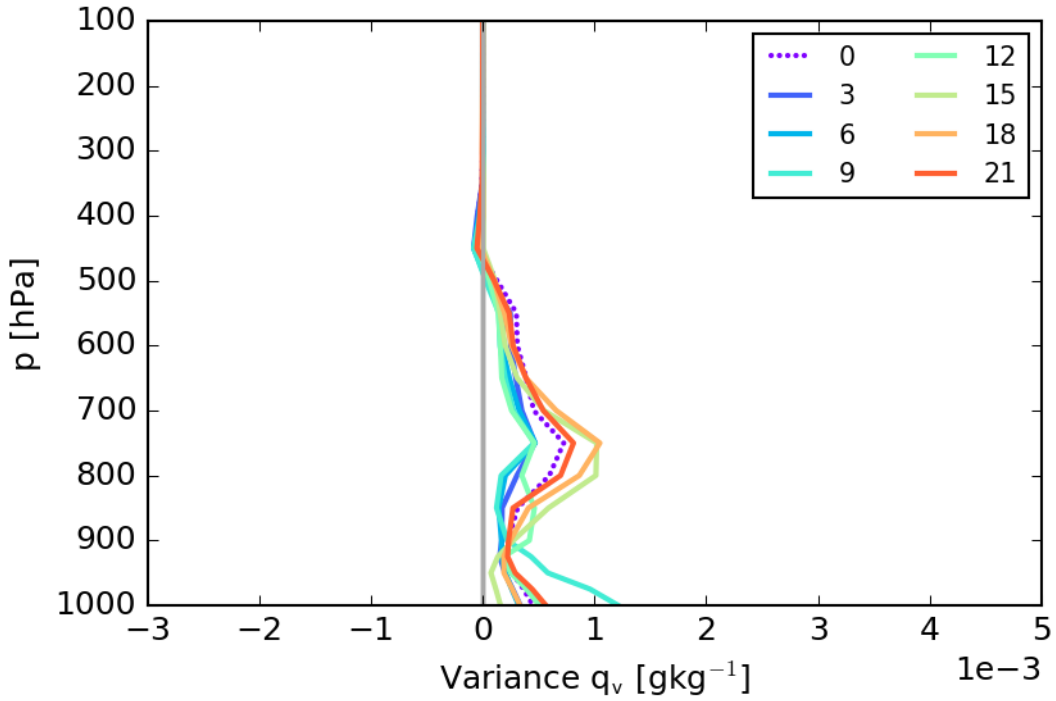

More organised convection would quite likely lead to more extreme values in q_v (i.e. drier in some regions and enhanced concentration of moisture in others), therefore the q_v variance in EXPL should be greater than in PARAM. The figure above displays the average differences in variance (EXPL – PARAM). What one can see here is an always positive difference with some diurnal cycle. This confirms the assumption of higher organisation. But this short analysis is too indirect in our eyes to be included in the article. Therefore we added on p14l24:

The latter is reflected in a larger variance of q_v throughout the lower and mid-troposphere in EXPL than in PARAM (not shown).

---

4. Use of commas:
I'm not a punctuation-expert, but I feel that there is a strong lack of commas throughout the manuscript. This distorts the flow and rhythm of reading. Examples are: p.3, L2 (season, low-level); p.4, L2 ((Sect 2.1), followed); p.6, L21 (set, ICON); p.7, L11 (given, concentrating); p.8, L8 (box, area-averaged); p.12, L9 ([...] Figure 4a), ranging); p.13, L32 (EXPL, but); p.16, L14 (Sect 3.2, contain); p. 25, L26 (maximum, changes); p.28, L3 (hPa, differences).

We tried our best to improve the punctuation throughout the paper, including your specific suggestions.

_____

More detailed comments:
p.1, L20-23: You should be a bit more specific here. Interactions of the WAM with the land surface? Representation of the hydrological cycle in West Africa?

The first statement is explained by the following two sentences, which enumerate some of the difficulties in modeling of the WAM system. We modified the first sentences to the following:

Modelling the West African monsoon (WAM) system is a challenge, as reflected for example in large disagreement in rainfall, surface air temperature and cloud cover between models participating in the Coupled Model Intercomparison Project phase 5 (CMIP5) (Roehrig et al., 2013). Climate and weather models show a considerable inter-model spread when studying for example the influence of sea surface temperatures (SSTs) on the WAM circulation (Xue et al., 2010; 2016; Rodriguez-Fonseca at al., 2015), interactions of the WAM with the land surface (Boone et al., 2009) or the representation of the hydrological cycle in West Africa (Meynadier et al., 2010; Poan et al., 2016).

---

p.2, L13: I don't understand what you mean with low-level processes. Do you mean boundary-layer processes or land-atmosphere interactions? Or do you already refer to the local factors and surface characteristics that are the topic of the next paragraph?

We added:

Several studies stress the importance of low-level processes, such as near-surface moisture advection or turbulent fluxes for the development of the WAM (Perill´e et al., 2016; Eltahir and Gong, 1996).

---

p.3, L4: What does "this phenomenon" refer to here? The low-level stratus or the NLLJ?

The evolution of the low-level stratus, which is connected to the low-level jet. We added:

Climate models struggle to realistically represent the diurnal cycle of the stratus in terms of cloud amount and occurrence as well as wind speed (Knippertz et al., 2011; Hannak et al., 2017).

> p.3, L7: I would remove the details of the radiative transfer model (âĂŽusing the two-stream radiative transfer model SOCRATES (Suite Of Community RAdiative Transfer codes based on Edwards and Slingo; Edwards and Slingo, 1996)')

Since the results can depend on the radiative transfer method that was used, we would like to keep this information. A delta-two-stream method could not account for radiative effects of cloud edges, for example.

> p.3, L13: What do you mean with "but feedbacks were not considered explicitly"? Where they not represented, or not analysed? Please clarify.

The sentence was modified to read "analysed" instead of considered.

> p.6, L13: Maybe again refer to Figure 1 here.

Done.

> p.7, L2: You haven't explicitly mentioned the control experiment yet. Maybe add a sentence on p.6, L19, saying that "f_op=1 corresponds to the control experiment."

Thank you! We added on p6,l29:

> f_op is varied from 0.1 to 10, where f_op=1 corresponds to the control experiment.

> p.8, Figure 2: I would suggest a few changes in this figure. I'd recommend using a white background for the maps and a different colour scale (e.g. the âĂŽYlGnBu' palette from https://betterfigures.org/2015/06/23/picking-a-colour-scale-for-scientific-graphics/). Furthermore, the DACCIWA box could be shown in every panel.

We modified the figure as suggested.

> p.9, L33: I don't really agree with the conclusion that ICON PARAM looks more consistent with the observations and ICON EXPL less. Together with CERES, ICON EXPL has a very good agreement with the few surface observations. This is in clear contrast to ICON PARAM, which tends to overestimate SSI compared to the surface observations. Maybe you can provide a more balanced conclusion of this paragraph.

You are right but ICON PARAM agrees better with the observations in terms of area-averaged solar surface irradiance, as explained in the respective paragraph:
"ICON EXPL shows the lowest SSI values with an area average of 164.7 W m^{-2} (Fig.\ \ref{solclim}a), much lower than PARAM with 191.6 W m^{-2} (Fig.\ \ref{solclim}b).
….
Evaluating this with observations is a challenge due to the many assumptions made in satellite-derived SSI and the few surface observations.
…..
In contrast, CERES does not seem to suffer from this problem due to a

different retrieval strategy (Fig.\ \ref{solclim}d). The box-averaged SSI is 188.4 Wm^{-2} and therefore very close to the ICON PARAM value, although with much less fine structure."

Therefore we change only the last sentence to clarify this:

> Overall this analysis demonstrates a significant observational uncertainty and suggests an overestimation of clouds in ICON EXPL leading to low average SSI, while ICON PARAM fields are more consistent with observations in this regard.

> p.9, L27-L29: Please clarify the sentence "brighter than the surface (except for snow) but in this region is likely still contaminated by clouds."

Due to the high reflection, cloudy pixels appear brighter than cloud-free pixels for a satellite, therefore the surface albedo can be determined from the lowest irradiance measurements. In the DACCIWA region, unfortunately, it is not easy to find a cloud-free irradiance in a specific pixel (usually one month of measurements is used to find the surface albedo, this has to be done for each pixel and each hour of day). We modified the explanation to make this clearer:

> As cloudy pixels appear brighter than cloud-free ones for SEVIRI, the surface albedo is estimated from the lowest irradiance measurement found per pixel in a given time period. In SWA, however, it is often difficult to find cloud-free scenes, leading to an overestimation of surface albedo (see also discussion of this problem in Hannak et al., 2017).

> p.12, L32: Depth of cloud modification layer: I thought you were modifying clouds below 700 hPa rather than below 750 hPa (see p.6, L13).

Well spotted. We corrected this to 700 hPa instead of 750.

> p.14, Figure 5: This figure has a relatively wild mix of colours and line types. Where applicable, I'd suggest to use more consistent colours throughout the paper, e.g. greenish colours for PARAM and reddish for EXPL (as in Figure 6). Further, I'd restrict the use of dashed lines in Figure 5 to the simulations with f_op=0.1.

We modified the Figure to be more clear and updated the figure caption accordingly.

> p.16, L24-26: I don't really understand what you want to say here. The convective parameterization is by design responsible for vertical moisture transport. But also explicit convection transports moisture in the vertical. So I don't understand how this would explain the lower sensitivity. Do you want to say that "the convective parametrization more efficiently transports moisture [...] compared to explicit convection."?

The parametrization scheme transports more moisture, than the explicit convection does. We modified the sentence to read:

To first order, the convective parametrization appears to transport moisture more efficiently out of the low- and mid-levels to deposit it into the convection-fed cirrus layer, as compared to explicit convection.

---

p. 19, L18 onwards: I don’t know exactly how TKE is treated in the parameterization, but as you say that the "mixing through convection is not reflected in TKE fields in PARAM“, it’s not surprising that the TKE profiles are very different. For me, the most striking difference between Figure 7 & 8 instead lies in the qc profiles. I would suggest some restructuring of this paragraph. It was also not always clear to me whether you are comparing PARAM and EXPL or the response to the opacity change for PARAM. This should be clarified.

We agree, and reviewer 1 commented on the same paragraph that was admittedly not easy to read. We restructured it as such (this time in green):

Figure 8 shows the corresponding profiles for PARAM. Despite the overall consistent signal in rainfall and radiation as documented in Fig. 4, there are many substantial differences between the two sets of experiments.

Despite a larger SSI (see Fig. 4a), PARAM has a lower daytime increase in near-surface temperature, particularly at 15 and 18 UTC, suggesting a possible impact of the earlier triggering of convection in PARAM (see Fig. 5). Near surface q_v (Fig. 8b) is strongly decreased at 09 UTC, probably due to the earlier onset of PBL mixing with transparent clouds, and then strongly increased at 12 and 15 UTC, possibly due to the lack of deep mixing as in EXPL, leading to very large differences between the two sets of experiments. Combined, the changes in temperature and moisture lead to overall less pronounced changes in RH at low levels (both negative near the surface and positive above; Fig. 8c), associated with mostly negative changes in q_c (Fig. 8e) except for 09 UTC. These explain the somewhat unexpected results for q_c discussed in the context of Figs. 7 and 6. In contrast to EXPL, PARAM operates a positive feedback mechanism, where a reduction in low cloud leads to a further reduction. This may clarify, why so many climate models show very large negative biases in cloud cover (Hannak et al., 2017).

Increased vertical mixing can be observed via TKE (Fig. 8d). Positive signals are restricted to the low levels during the day (09, 12 and 15 UTC), with the latter time showing indications for increased mixing reaching midlevels. All hours from 18 UTC to 09 UTC show decreased TKE below 600 hPa and hardly any change at all above that. One needs to bear in mind, however, that the mixing through convection is not reflected in TKE fields in PARAM. Nevertheless, the PARAM signals, at least at low levels, are in clear contrast to EXPL (Fig. 7d) where TKE increases everywhere. These differences are strong indicators that the interplay between PBL turbulence, shallow and deep convection fundamentally differs between the two model configurations. Particularly during nighttime, PARAM shows a slight stabilization in the temperature profile (Fig. 8a) above 925 hPa that appears to suppress turbulence generation in this layer. This cooling may be related to the enhanced NLLJ (Fig. 8f), but it is not clear why this effect does not work in EXPL, where an even more enhanced NLLJ and also a stabilization is observed (Figs. 7a and f). The change in mixing have profound impacts on many low-level fields, whereas more agreement between EXPL and PARAM is found at mid- and upper-levels, except for some changes in the diurnal cycle.

> Overall this discussion demonstrates the enormous importance of vertical transport and mixing in a moist tropical environment where the PBL, low clouds and deep convection are closely coupled through radiative effects.

> p.21, L3: You didn't state the sign of the modification of low clouds, but then say that it leads to substantial increases in precipitation. I'd suggest to reformulate the sentence as follows: "[..] how moderate reductions in low-cloud opacity [...]".

Done as suggested.

> p.22, L7: I wouldn't use the word "impressive" here, especially as you stress in other parts of the manuscript that a quantitative interpretation of the results is questionable. Maybe just use "an increase of 560%". The same is true for p.30, L13 ("an impressive factor of 5!"). I also don't really like the use of the word 'enormous' (e.g. p.25, L24; or p.31, L26), but that might be a matter of taste.

We deleted the adjective impressive in "in the northern half of the DACCIWA box corresponds to an impressive 560%, while the southern half... " but kept it in the sentence "Particularly in the northern half of the modification region, rainfall increases by an impressive factor of 5!" because it should stress the strong effect that this small modification causes. We replaced the first enormous by a more neutral "large" but kept the second "enormous" because we think it to be appropriate in the given context.

> p.22, L31: I don't see how the sentence "This may explain the general tendency..." fits in the discussion of the EXPL simulation here, as I assume that this might be different between explicit and parameterized convection.

In climate models, we found for this region in Hannak et al. (2017) that a too strong developed nocturnal low level jet is connected to a too low cloud cover. The discussion in the respective paragraph in our paper may give hints on the processes and explain why this happens, which could be used as an explanation for climate models, too. But you are right, since the convection is parametrized, other factors can be involved, too. Therefore, we modified the paragraph as such:

> Assuming a similar behaviour also in models with parametrized convection, these processes may explain, why an underestimation of low clouds is often found together with an overestimation of NLLJ for many climate models (Knippertz et al., 2011; Hannak et al., 2017), but this needs further study.

> p.27, Figure 13: Change legend in panel (e) to f_op=1.0 & f_op=0.1.

Thank you for spotting this!

> p.28, L 13-14: I don't understand what you mean with "effectively removing tropospheric surplus and depositing...", maybe something is missing here?

We added “surplus moisture”.

---

p.30, L21: I would assume that air advected from the ocean is moist, not dry. Am I missing something here?

Due to the cold temperatures and subsidence over the ocean at this time of the year, the advected air from the ocean is in fact drier than air that has already resided over land (Schuster et al., 2013)! We added “dry subsided air from the ocean” to make clearer how this is possible.

S1, p.1, L27-29 and Figure S1: maybe add a measure of spread between the different runs to indicate the variability.

Done.

Typographic suggestions:

p.2, L7: and ITD shift –> and the ITD shift

Done.

p.2, L14: Eltahier –> Eltahir

Done.

p.3, L4: Omit either realistically or correctly.

Done.

p.5, L23: allows –> allow

Corrected.

p.5, L24: terrain following –> terrain-following

Done.

p.6, L21: remove grid ("a grid spacing of 13.2 km grid...“)

Done.

p.7, L3: first (Sect. 3.1) –> first section (Sect. 3.1)

Done.

p.7, L17-L18: add a "the“ in front of "adjacent ... highlands“

Corrected.

p.9, L1: "by on the order of“ –> by about

Corrected.

p.12, L18: from –> of

Done.

p.13, L21: following –> followed

Corrected.

p.14, L4: clod –> cloud

Done.

p.16, L5: by on the order –> by about

Done.

p.16, L8: with values –> with absolute increases

Corrected.

p.16, L18: remove "than“

Done.

p.16, L18: results –> result

Corrected.

p.19, L18: hardly any change at all above –> hardly any change above

Done.

p.22, L26: with values –> with decreases

Done.

p.25, L32: aerosol-radiation or –cloud interaction –> aerosol-radiation or aerosol-cloud interaction

Corrected.

p.28, L21: impacts on higher and –> impacts on higher levels and

Done.

Reply to referee #1

We would like to express our gratitude for the insightful review of our study. The discussion is very helpful and gives insightful remarks and valuable recommendations. We took them into account while preparing the revised version of the manuscript.

Below, the actual comments are given in blue color.
The text added to the revised version of the manuscript is marked in green.

> Major Comments:
> While the explanation of how the clouds were altered in the model was very clear and innovative, I have several comments about the general setup of the model and how the simulations were performed and analyzed.
> First, why was the ICON model used, and more specifically, why was a global model used for this experimental setup? For such short runs, I would think a regional or at least a nested global model would be sufficient. You state that computational cost limited your runs.

The ICON model has now become a standard tool in atmospheric science in Germany following a seamless concept (one model frame for LES, NWP and climate modelling). It is widely used both by the national weather service and by many university researchers. Forecasts from ICON have been evaluated with DACCIWA campaign observations (separate paper in preparation). As a recently developed model, it fulfills highest standards and runs very efficiently. We agree that a regional model would have been sufficient here but the very flexible nesting capability of ICON allowed us to avoid any undesirable effects at the model boundaries. A classical limited area version of ICON that could be driven with existing ICON global data is currently in preparation but did not exist when we started the study. Therefore we tested the global ICON model with a nest and found that it performed well in our test cases. We also like to stress that computational cost was not the main limiting factor for the analysis, but the large amount of data, even though we restricted the output to West Africa.
We included a short explanation on p6l11:

> Currently ICON is only configured as a global model but its high flexibility in terms of one- and two-way nesting allows a regional focus without any undesirable boundary effects sometimes observed for traditional limited-area models. It performed well compared to ERA Interim (ERA-I hereafter) in several test cases we ran for DACCIWA. The comaprison can be found in the supplementary material. The simulation period was not so much limited by computational cost but by the large amount of output, since many different state variables had to be saved for the analysis.

> Do you used fixed SSTs or an interactive ocean (or ocean surface)? Since the simulations are so short, I don't expect the treatment of the ocean surface to have much effect, but it would be good to know.

SSTs are contained in the input conditions, but they are not updated during run-time. We also did not expect a strong effect because of the short simulation times. We added to the sentence on p31l12:

> Note that in the NWP simulations SSTs stay largely constant during the short run time; they are initialised with ERA-I, but not updated during a 5-day simulation.

> For the EXPL runs, what is the domain of the nested grid? This is probably unimportant, but could have implications as odd things can happen on the boundary between nested grids.

We tested this and asked DWD for advice (to be on the safe side) and chose the grid large enough. The innermost grid was circular (this fitted best to the ICON base grid, which covers the earth in triangles). It had a radius of 30 degree and was centered on 0°E and 13°N. This way, it covered large parts of North-Western Africa. We added on p7l7:

> The nest has a circular domain centered on 0° E and 13° N with a radius of 30° such that it is large enough to avoid undesirable effects near the nest's boundary.

> Finally, what period is the data analysis averaged over? Is it the final four days of the five day simulations? This would be congruent with five day simulations having a single day overlap when the model was started every fourth day, however, it should be clearly stated.

Yes, that's true. We added on p8l4:

> The averages were created from the final four days of the five day simulations.

> Is this period the same for analysis of both the local and regional response?
> The timescale of the local and regional response is an important factor in interpreting your results, so you should clearly state your averaging period for analysis and support your choice with evidence from your simulations (as in the supplementary material) and/or the literature.

The averaging period is the same for the local and the regional response. We did not change any setting in between in order to keep the two responses comparable.
We added on p22l7:

> To answer these questions, we expanded the analysis of the sensitivity experiments and included the Sahel zone up to about 25° N.

> When describing the ICON model base state and comparing it to obs and reanalyses it may be helpful to also know how the control simulations compare with the obs/reanalyses/Hannak et al. In terms of cloud fraction and LWP/IWP. Is it a model that produces a reasonable amount of low level clouds in the base state? The discussion on pages 8 and 9 somewhat address this, but since the paper is on clouds, it might be nice to just state how the control simulations cloud fields compare to obs/reanalyses.

We looked at that and compared the profiles of low-level cloud cover, LWP, and wind speed to ERA-I. We found the base state to be satisfactory in our study region and wrote a paragraph about this. However, because the article became too long, we decided to remove it again. Now we have put a figure into the supplementary material and describe it as follows:

In addition to the general characterization of the meteorological conditions in southern West Africa for the variables precipitation and radiation, a brief discussion about the diurnal cycle of the vertical atmospheric structure is given for the wet monsoon season July, August and September 2006.
Comparison of ICON CLIM with ERA-I and observations confirms the applicability of the ICON model for the sensitivity experiments of the main article.

Figure S1 shows average profiles of cloud cover (CLC), relative humidity (RH), horizontal wind speed v_horiz as well as specific cloud water content q_c for 00, 06, 12 and 18 UTC (corresponding to local time in our study region). At 00 UTC the NLLJ is already well established and the low-level cloud deck is beginning to form (Fig. S1a).
ICON shows a considerably stronger jet than ERA-I reaching 7 m s^{-1} at 925-950 hPa and consistently lower values in CLC, RH and q_c. In contrast to ERA-I, ICON tends to concentrate cloud water in the upper parts of the cloud deck around 850 hPa.
The relatively small differences in RH between the two datasets (more than 90\% from 830 hPa downwards) in contrast to differences in CLC and q_c illustrates a substantial sensitivity to the subgrid-scale cloud scheme or possibly differences in spatial variance of RH, as the dependance of CLC on RH is quadratic in ICON. The tendency of stronger NLLJ and less cloud was also found in many climate models (Hannak et al. 2017). At midlevels around 560 hPa ICON shows a secondary peak in v_horiz, CLC, RH and q_c not found in the overall smoother and moister ERA-I profiles.

At 06 UTC the NLLJ is very similar to 00 UTC but the low-level cloud deck increases markedly in cover and q_c accompanied by an increase in RH to values well above 95 % below 900 hPa (Fig. S1b). Maximum CLC occurs at 950 hPa reaching 25% in ICON and about 45% in ERA-I, which is more realistic (cf. van der Linden et al., 2015).
Overall the discrepancies between the two models are qualitatively similar to 00 UTC (Fig. S1a). At midday (Fig. S1c), radiative heating lifts and dissolves the low-level cloud deck shifting the maximum in CLC and RH to 850 hPa, where a pronounced peak in q_c develops. Surface heating and turbulent mixing markedly slows down the low-level jet (e.g. 4.5 m s^{-1} in ICON) and decreases RH to under 90% below 900 hPa with ICON being substantially drier and less cloudy in that layer.
Finally at 18 UTC (Fig. S1d) the low-level jet starts re-accelerating, keeping the generally higher values in ICON found at all times of day. The deep daytime mixing has reduced CLC and q_c and created an almost vertically constant offset between the two modeling systems. RH is already increasing at this time of day, particularly in ICON, where also the sharp gradient in v_horiz suggests a beginning decoupling of the surface. Such an early evening transition is consistent with observations as documented in Fig. 3d in Schuster et al. (2013).
The comparison between the two datasets shows considerable biases at all times of day with generally higher low- and midlevel wind maxima in ICON but moister and more cloudy low levels in ERA-I. Investigating the reasons for these discrepancies is beyond the scope of this paper but the overall agreement in vertical structure and diurnal cycle suggests that sensitivities tested with ICON should be qualitatively meaningful.

The entire paragraph at the end of Page 12 and beginning of Page 13 is a bit confusing and unclear. (Page 12, Line 26 through Page 13, Line 5) Why do you connect the discrepancy in the longwave component with a dynamical response, but not the discrepancy in SSI? Could the change in upper-level clouds account for this difference? It is important to point out that July 2006 might not have been the most average year, but I'm a bit perplexed by why that can explain SSI and not OLR. Maybe I'm missing

something here.

The main point was to find out, how much of the change in cloudiness could be attributed to the dynamical response in the fully non-linear model as compared to the radiative effect of the static cloud cover itself. Therefore we compared with the study by Hill et al. that only takes the latter into account. Unfortunately it is not easy to compare, because the time periods considered are not the same. This is why the characteristics of July 2006 relative to the climatological context matter. In addition, of course, clouds simulated by ICON can deviate from what CERES sees in reality. Therefore we did not make a statement about SSI because it is not possible to disentangle the two problems. For longwave is easier to interpret because there are qualitative changes (the changing sign of the variation in OLR).

We reworded the section on p13l25 to read:

> The most plausible explanation is that the relatively dry July 2006 had overall less mid- and high-level clouds than the June–September 2006–2010 average used in Hill et al., leading to a largely consistent but relatively larger effect of modifying low-level cloudiness (consistent with Fig. 9 in Hill et al., 2018). This makes it hard to distinguish the purely radiative signal from the fully nonlinear dynamical response of the atmosphere. The latter is more distinguishable in the longwave component. The increase in deep convection with optically thinner low clouds in ICON PARAM leads to a decrease in OLR in the model on the order of 10 W m−2, while the radiative transfer calculations by Hill et al. show even a small increase. In contrast, for SLI the purely radiative
> effect is a marked decrease, but ICON-PARAM shows almost constant SLI, likely due to combined dynamical effects of the increase in low-level temperature, deep convective clouds and column moisture (see Fig. 12).

> Page 19, Line 15: “most striking” is a bit subjective, don’t you think? I agree that it is very striking, but I was immediately more intrigued by the low level qv and qc, whose signals can be interpreted as due to changes in vertical mixing, some of which can be explained by TKE. I think describing and explaining the signals in this manner might be more causal, but this, I suppose, is more personal opinion. This is also a massive paragraph and could probably be broken up between these two features.

Reviewer 2 said exactly the same, so we rephrased it and tried to restructure the paragraph to be more readable.

> Figure 8 shows the corresponding profiles for PARAM. Despite the overall consistent signal in rainfall and radiation as documented in Fig. 4, there are many substantial differences between the two sets of experiments.
>
> Despite a larger SSI (see Fig. 4a), PARAM has a lower daytime increase in near-surface temperature, particularly at 15 and 18 UTC, suggesting a possible impact of the earlier triggering of convection in PARAM (see Fig. 5). Near surface q_v (Fig. 8b) is strongly decreased at 09 UTC, probably due to the earlier onset of PBL mixing with transparent clouds, and then strongly increased at 12 and 15 UTC, possibly due to the lack of deep mixing as in EXPL, leading to very large differences between the two sets of experiments. Combined, the changes in temperature and moisture lead to overall less pronounced changes in RH at low levels (both negative near the

surface and positive above; Fig. 8c), associated with mostly negative changes in q_c (Fig. 8e) except for 09 UTC. These explain the somewhat unexpected results for q_c discussed in the context of Figs. 7 and 6. In contrast to EXPL, PARAM operates a positive feedback mechanism, where a reduction in low cloud leads to a further reduction. This may clarify, why so many climate models show very large negative biases in cloud cover (Hannak et al., 2017).

Increased vertical mixing can be observed via TKE (Fig. 8d). Positive signals are restricted to the low levels during the day (09, 12 and 15 UTC), with the latter time showing indications for increased mixing reaching midlevels. All hours from 18 UTC to 09 UTC show decreased TKE below 600 hPa and hardly any change at all above that. One needs to bear in mind, however, that the mixing through convection is not reflected in TKE fields in PARAM. Nevertheless, the PARAM signals, at least at low levels, are in clear contrast to EXPL (Fig. 7d) where TKE increases everywhere. These differences are strong indicators that the interplay between PBL turbulence, shallow and deep convection fundamentally differs between the two model configurations. Particularly during nighttime, PARAM shows a slight stabilization in the temperature profile (Fig. 8a) above 925 hPa that appears to suppress turbulence generation in this layer. This cooling may be related to the enhanced NLLJ (Fig. 8f), but it is not clear why this effect does not work in EXPL, where an even more enhanced NLLJ and also a stabilization is observed (Figs. 7a and f). The change in mixing have profound impacts on many low-level fields, whereas more agreement between EXPL and PARAM is found at mid- and upper-levels, except for some changes in the diurnal cycle.

Overall this discussion demonstrates the enormous importance of vertical transport and mixing in a moist tropical environment where the PBL, low clouds and deep convection are closely coupled through radiative effects.

The first panel in Figure 9 is really fantastic! However, I feel that the aspect of it that discusses the differences between ICON and TRMM as well as the description in the text (Page 21, Line 10 through Page 22, Line 1 “As already discussed . . . gap between the rainfall maxima”) should be moved to Section 3.1 where you are discussing the differences in the control simulations and the TRMM. When inserted here it subtracts from the main point of the section which is to show how the perturbation effect precipitation into the Sahel.

Thank you. We agree that it distracts from the main topic and inserted the averages into figure 2, where the description was already given. We added the following lines:

The small middle panels in Fig. 2 show the rainfall dependent on latitude but averaged over 8° W-8° E as further analysed in section\ \ref{precip3}. The rainfall maxima over the Niger Delta region and along the coast of Guinea, Sierra Leone and Liberia are not captured in this average, which explains the rather small values between 7-10° N.

We kept the first panel in Figure 9 because it is important for the reader to see the absolute decline in rainfall when traveling northwards.

Page 22, Line 11: “This may suggest that modulations to the WAM allow a slightly deeper penetration of rainfall into the continent but one month is probably too short to make any definite statements on this area.” I am a bit confused by this statement. You

> are suggesting that only looking at July 2006 might not be enough to make a robust statement?

We agree that this is a bit misleading and reworded the passage to now read:

> However, given that in the northern Sahel rainfall is usually caused by few distinct, intense convective systems and that soil moisture perturbations become increasingly important, five-day simulations during one month is probably insufficient to make any definite statements for this area.

> Page 25, Lines 32-34: “An interesting implication . . . no significant regional impacts.” This statement makes it sound like you are generalizing your result to other regions, how do you support that claim? Or are you focusing on the response to just altering the clouds in the DACCIWA region? Your statement in the summary (beginning Page 31, Line 10 with “Therefore these results . . .”) is much more well supported.

Here we refer only to the DACCIWA region, we made this clearer and the lines read now (on p27l1):

> An interesting implication of this result is that whatever change in aerosol-radiation or aerosol-cloud interaction is caused through changes in anthropogenic emissions in the DACCIWA region, it will likely have measurable local impacts but probably no significant ramifications elsewhere.

> Page 28, Lines 18-22: This paragraph feels out of place. Why are you concerned with how quickly the atmosphere returns to its normal state? The statement “impacts on higher and more remote regions can last days” is misleading as the supplemental material suggests that the residual impacts on remote regions are complicated by the chaotic nature of the atmosphere. I think the plot in the supplemental material is quite interesting and helps explore the timescales of the response, as well as the persistence of changes when the altered clouds are removed. It might be useful to plot the envelop of the anomalies in Figure S1, in order to show the variability between the ensemble members. This would help clarify what is a consistent response to the forcing and what is due to internal variability.

The original idea was to find out, if the experiment that we conducted has a long-lasting effect on the structure of the atmosphere, or if it is a short-lived phenomenon. In the first case, an influence on remote regions would appear more likely. We agree that the chaotic nature of the system makes it difficult to discuss the life-time effect. We plotted the respective figure again and included the envelope in the bias. Since the envelope stays quite constant with time after the switch-off for the boundary layer variables, we believe that our statements are correct. We modified the passage on p29l24 in the main manuscript in the following way:

> Impacts on higher levels and more remote regions can last for days but the signals hardly stand out from the high level of background variations indicating the chaotic nature of the atmosphere.

And in the supplementary material in the figure caption of Fig. S1:

> The corresponding differences are shown as green lines in (f)--(j), where the shaded area denotes the maximum and minimum values of the time-series.

And added to the corresponding text on p4l13 Where we had already referred to the chaotic nature of the system:

> The latter is reflected in the growing shaded areas denoting the envelope of all runs in the bias in the right-hand side panels of Fig. \ref{longr}.

> What is the remote (Sahel) response of precipitation for the positive values of f_op = 3 and 10 in the PARAM experiments? I realize these are extreme values, but it would be interesting to see if the same signals appear.

In the Sahel there is not too much difference noticeable due to the already low absolute values of precipitation. The DACCIWA-box, on the other hand, dries out further as already indicated in Fig. 4c. Below please find a figure (middle panel control run, right panels f_op = 3, left panel f_op=0.1) that illustrates the regional distribution of this drying.

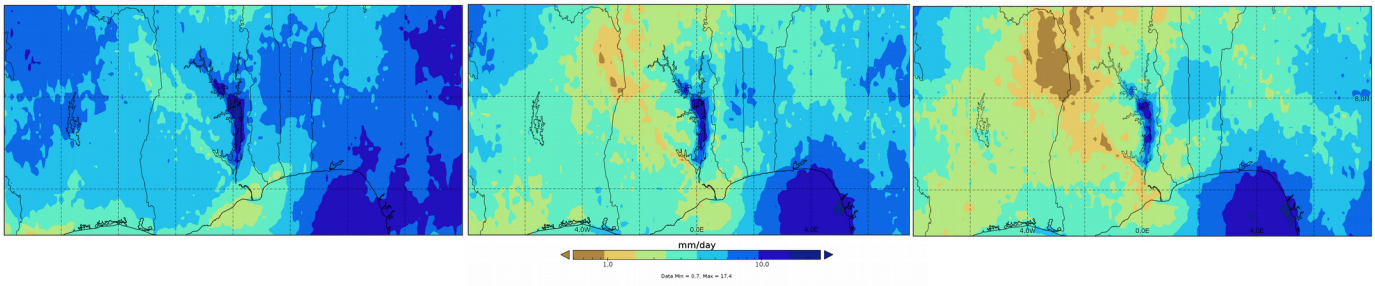

and the same plot as figure 9 in the paper, but with f_op=3 and f_op=10 included:

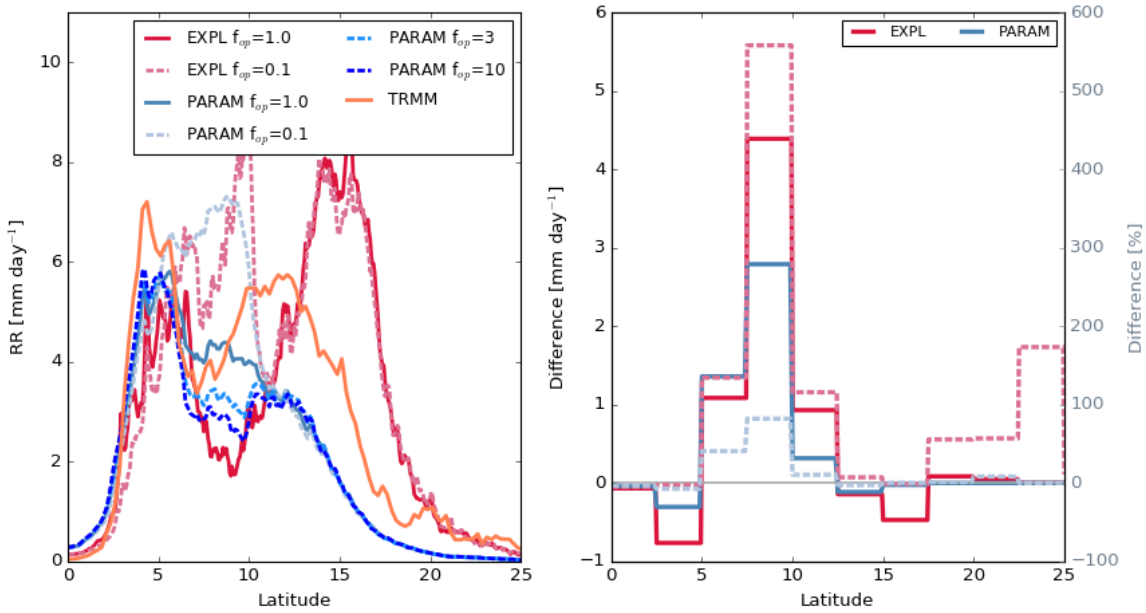

Minor Comments & Typographic Corrections:
Many passages would be improved by the introduction of commas, especially the Oxford comma. I've identified a few below, but if you'd like, I would be glad to mark up the submitted manuscript with where I believe commas would help separate clauses and help clarify the manuscript.

Thank you, we tried our best to improve the punctuation.

Page 1, Line 7: effect

Done.

Page 1, Line 24: "do not show skillful forecasts of precipitation for the next days", is awkward, perhaps "do not produce skillful short term precipitation forecasts" is clearer.

Agreed.

Page 2, Line 9: "determined by the WAM system", is unclear, what about the WAM system determines these characteristics? "are connected within the WAM system" emphasizes the challenge of the interconnectedness of the WAM.

That's better, thank you.

Page 2, Line 32: I would remove "which is currently gaining increasing attention".

Done.

Page 3, Line 17: misrepresenting

Done.

Page 3, Lines 19-30: I would reorganize this entire paragraph to flow better.
This study is part of the Dynamics-Aerosol-Chemistry-Cloud Interactions in West Africa (DACCIWA) project (Knippertz et al., 2015) that aims to better understand the consequences of the rapid increase of anthropogenic emissions in West Africa on the local air quality, weather and climate. To the best of our knowledge, it is the first to analyze the radiative impact of the low-level cloudiness over southern West Africa on the thermodynamics and dynamics of the regional atmospheric system in a fully non-linear and systematic way. The analysis is based on a number of targeted sensitivity experiments using the numerical weather prediction model ICON (Icosahedral Nonhydrostatic), systematically changing the optical thickness of the model clouds. This allows us to clarify the impact of the inter-model spread in cloudiness found in Hannak et al. (2017) on the overall monsoon development in both parameterized and explicit regimes of convection. Although aerosols are not directly modeled in our experiments, the effects found for imposed changes of cloud optical thickness also help to understand variations of the natural system brought about by aerosol effects on cloud properties and radiation, which in a similar way control the amount of shortwave radiation reaching the surface or interact with clouds through modifications in the diurnal cycle of the PBL (e.g. Deetz et al., 2018a).

Thank you so much, this is really appreciated and we put it into the manuscript.

Page 6, Line 4: Green's

Done.

Page 6, Line 7: (Dee et al., 2011), and do not use data assimilation. (the comma helps separate the idea that the simulations are not using assimilation instead of ERA-I,

which clearly does)

Done.

Page 6, Lines 10-11: Initializing ICON runs at 00 UTC would mean starting the runs in
during the development phase of the low-level clouds and therefore the runs were initialized at 12 UTC. ("would mean to start directly" is awkward and "preferred" makes it unclear that the runs were in fact started at 12 UTC)

Thank you.

Figure 2: maybe outlining the box in each subplot would help highlight the similarities and differences

Since reviewer #1 had an issue with this figure, it was modified and now contains a box in each subplot.

Page 9, Line 11: remove "Similar to Fig. 2" it's not needed

Done.

Figure 4: why is the axis dimension for SLI so large? All the other subplots are so well framed, but this one has so much empty space it looks weird. Maybe 400-430 W/mˆ2 would suffice?

That was actually done on purpose. The range is similar to the other radiative quantities to illustrate that the variability is not so large for SLI. Therefore, we would like to keep it this way.

Page 12, Line 6: How do the fully nonlinear processes represented in the ICON . . .

Done.

Page 12, Line 26: I feel this might read better as: "The simple linear model used by Hill et al. (2018) allows a rough estimate of how much of the change in the ICON radiative fluxes are due to direct . . . "

Done.

Page 12, Line 29: I think it would be more proper to not capitalize "Increases" after the colon, to signify that it is not a sentence fragment. Usually, you should only capitalize the first word after a colon if the clause is independent.

Done.

Page 16, Line 23: equal to

Corrected.

Figure 10: The legend for subplot (e) should have fop = 0.1 for the red curve.

We totally overlooked that, thank you!

Page 24, Line 4: south-north profiles of Figs. 10a-c for each hour

Done.

Page 26, Line 1: There needs to be a better transition here. Begin with a clear sentence that you are shifting back to looking at the PARAM simulations and why, before introducing the figure.

We added on p27l3:

This quite noticeable impact was found in the simulations with explicitly simulated convection. The influence of parametrization of convection in this experiment will be discussed next.

Page 28, Line 9: remove “just mentioned”

Done.

Section 4, First Paragraph: The second sentence introduces the idea of representation of clouds in models, but then immediately returns to the idea of describing the clouds in reality. The paragraph might flow better this way:
In the present study, we analyzed the role of low-level clouds over southern West Africa on the local meteorology and larger monsoon system. They frequently form during the night close to the surface and often persist long into the following day. At their maximum diurnal extent, they cover a vast area of about 850 000 km2 in southern West Africa (van der Linden et al., 2015). Their formation is linked to cold advection and turbulent mixing associated with the NLLJ and radiative cooling (Schrage and Fink, 2012; Schuster et al., 2013; Kalthoff et al., 2018). These clouds play an important role in the energy budget and diurnal cycle during summertime and tend to be badly represented in many climate models (Hannak et al., 2017). The role of these clouds in the WAM system was assessed here for the first time in a fully nonlinear way via sensitivity experiments using the ICON model from the DWD in NWP mode for July 2006.

We would like thank you very much for this rephrasing, we changed the paragraph accordingly.

Supplemental Material, Page 1, Line 4: Would read better as: “To investigate this we use EXPL experiments, in which f_op = 0.1 is applied for the first 4 days . . .” The phrase “as in EXPL” makes it unclear what type of experiment is being done here.

Thank you, we adapted it.

The role of low-level clouds in the West African monsoon system

Anke Kniffka[1], Peter Knippertz[1], and Andreas H. Fink[1]

[1]Institute of Meteorology and Climate Research, Karlsruhe Institute of Technology, Karlsruhe, Germany

Correspondence to: Anke Kniffka (anke.kniffka@kit.edu)

Abstract. Realistically simulating the West African monsoon system still poses a substantial challenge to state-of-the-art weather and climate models. One particular issue is the representation of the extensive and persistent low-level clouds over southern West Africa (SWA) during boreal summer. These clouds are important in regulating the amount of solar radiation reaching the surface but their role in the local energy balance and the overall monsoon system has never been assessed. Based on sensitivity experiments using the ICON model for July 2006, we show for the first time that rainfall over SWA depends logarithmically on the optical thickness of low clouds, as these control the diurnal evolution of the planetary boundary layer, vertical stability and finally convection. In our experiments, the increased precipitation over SWA has small direct effect on the downstream Sahel, as higher temperatures due to increased surface radiation are accompanied by decreases in low-level moisture due to changes in advection, leading to almost unchanged equivalent-potential temperatures in the Sahel. A systematic comparison of simulations with and without convective parameterisation reveals agreement in the direction of the precipitation signal but larger sensitivity for explicit convection. For parametrized convection the main rainband is too far south and the diurnal cycle shows signs of unrealistic vertical mixing, leading to a positive feedback on low clouds. The results demonstrate that relatively minor errors, variations or trends in low-level cloudiness over SWA can have substantial impacts on precipitation. Similarly they suggest that the dimming likely associated with an increase in anthropogenic emissions in the future would lead to a decrease of summer rainfall in the densely populated Guinea Coastal area. Future work should investigate longer-term effects of the misrepresentation of low clouds in climate models, e.g. moderated through effects on rainfall, soil moisture and evaporation.

1 Introduction

Modelling the West African monsoon (WAM) system is a challenge, as reflected for example in large disagreement in rainfall, surface air temperature and cloud cover between models participating in the Coupled Model Intercomparison Project phase 5 (CMIP5) (Roehrig et al., 2013). Climate and weather models show a considerable inter-model spread when studying for example the influence of sea surface temperatures (SSTs) on the WAM circulation (Xue et al., 2010; 2016; Rodriguez-Fonseca at al., 2015), interactions of the WAM with the land surface (Boone et al., 2009) or the representation of the hydrological cycle

in West Africa (Meynadier et al., 2010; Poan et al., 2016). Current numerical weather prediction (NWP) models do not produce skillful short term precipitation forecasts (Haiden et al., 2012, Vogel et al., 2018).

The climate of West Africa is to a large extent controlled by the WAM (Hall and Perrilé, 2006; Fink et al., 2017). The monsoon is connected to the large north–south pressure gradient between higher pressure over the Atlantic cold tongue (Caniaux et al., 2010), which develops during March to May, and the Saharan heat low forming due to the enhanced insolation in northern hemispheric summer. The onset of the monsoon in June (Fitzpatrick et al., 2015), which often occurs abruptly (Sultan and Janicot, 2000), is accompanied by an increase in southwesterly inflow from the tropical Atlantic and a northward shift of the main rain band and the Intertropical Discontinuity (ITD), the airmass boundary between cool monsoonal and hot and dry Saharan air. The rain band reaches its maximal northern position in August/September, after which the rainband and the ITD shift southward again. Due to this characteristic seasonal behaviour, local variations in rainfall, winds, temperature and clouds are connected within the WAM system (Thorncroft et al., 2011). Eltahir and Gong (1996) developed a theoretical framework for the driving forces of the WAM describing it as a direct thermal circulation for moist atmospheres. They found that the gradient of entropy in the planetary boundary layer (PBL) is a key factor for the strength of the monsoon circulation and its inter-annual variations. Using a simple 2D-model, Zheng et al. (1999) argue that an increase of net surface radiation leads to an increased entropy and thus a stronger WAM circulation. Several studies stress the importance of low-level processes, such as near-surface moisture advection or turbulent fluxes for the development of the WAM (Perillé et al., 2016; Eltahir and Gong, 1996).

Variability within the WAM and day-to-day changes are determined by more local factors such as surface characteristics and incoming solar radiation (Lafore et al., 2017; Taylor et al., 2011) or specific regional features such as orography or the land-sea breeze. Lavender et al. (2010) studied soil-moisture and land-atmosphere coupling for the 15-day westward-propagating mode of intraseasonal variability of precipitation and wind, and found that soil moisture plays an active role in the development of the WAM system. Propagating synoptic-scale disturbances such as African easterly waves or single vortices can lead to marked variations in rainfall (Diedhiou et al., 1999; Knippertz et al., 2017). A key process for many aspects of the WAM is moist convection, which occurs in a wide range of degrees of organization depending on ambient thermodynamic conditions and shear (Maranan et al., 2018). Marsham et al. (2013) demonstrated that the use of a convective parameterization can lead to substantial errors in the diurnal cycle of precipitation, cloudiness and the entire monsoon circulation due to differences in both latent and cloud radiative heating. Couvreux et al. (2014) assessed the diurnal cycle of thermodynamics in the lower troposphere in four contrasted regimes over West Africa. The NWP models they analyze suffer from an erroneous surface-atmosphere-cloud coupling on short time scales, leading to false cloud cover, particularly in the lower parts of the atmosphere. Not limited to West Africa, Noda et al. (2009) show that sub-grid cloud processes in the Non-Hydrostatic Icosahedral Atmospheric Model (NICAM) influence not only the development of low-level cloudiness but also middle and higher clouds, even at horizontal grid scales of 14 and 7 km due to differences in turbulent transport. Also different radiation schemes have been found to impact on precipitation and the north-south gradient of surface temperature, which affects the strength of the monsoon flow (Li et al., 2015).

An interesting local to regional-scale feature, is the low-level stratiform cloud cover in southern West Africa that develops at night-time and persists long into the following day (Knippertz et al., 2011; Schrage and Fink, 2012; Schuster et al., 2013). Due to this persistence, the radiative characteristics of these clouds influence the PBL development at the Guinea Coast and further inland. Its formation is connected to the evolution of the nocturnal low-level jet (NLLJ; Schrage et al., 2007) and involves advection of cool air from the ocean, radiative cooling and turbulent mixing associated with the NLLJ (Schuster et al., 2013; Adler et al., 2017). During the monsoon season, low-level stratus occurs frequently with typically less than a third of all nights being cloud-free at a given location (Schrage and Fink, 2012; van der Linden et al., 2015; Kalthoff et al., 2018). Climate models struggle to realistically represent the evolutionary cycle of the stratus in terms of cloud amount and occurrence as well as wind speed (Knippertz et al., 2011; Hannak et al., 2017). Hill et al. (2018) studied the radiative impact of different cloud types in this region with detailed radiative transfer calculations based on the CERES-CloudSat-CALIPSO-MODIS dataset (Ham et al., 2017) using the two-stream radiative transfer model SOCRATES (Suite Of Community RAdiative Transfer codes based on Edwards and Slingo; Edwards and Slingo, 1996). They find that low-level clouds have a cooling effect, the magnitude of which depends on the overlying midlevel and high clouds. Ignoring low-level clouds (defined as below 680 hPa by Hill et al.) but keeping all other clouds the same would lead to errors of about 35 Wm^{-2} for downwelling surface solar irradiance (SSI) and -25 Wm^{-2} for outgoing shortwave radiation (OSR) at the top of the atmosphere (TOA). Knippertz et al. (2011) indeed found that the lack of low-level cloudiness in climate models leads to an overestimation of SSI compared to station measurements but feedbacks were not analysed explicitly. It can be expected that increased surface heating due to a lack of low clouds should lead to a deeper PBL and possibly more convection, which may significantly redistribute moisture vertically. This would be consistent with recent findings by Deetz et al. (2018a), who demonstrate significant sensitivity in PBL height and daytime stratus-to-cumulus transition to aerosol radiative effects. In addition, misrepresenting low clouds is likely a source of error in the simulated moisture budget (Schrage and Fink, 2012), which together with SSTs controls the WAM development to a large extent (Xue et al., 2010; 2016).

This study is part of the Dynamics-Aerosol-Chemistry-Cloud Interactions in West Africa (DACCIWA) project (Knippertz et al., 2015) that aims to better understand the conse- quences of the rapid increase of anthropogenic emissions in West Africa on the local air quality, weather and climate. To the best of our knowledge, it is the first to analyze the radiative impact of the low-level cloudiness over southern West Africa on the ther- modynamics and dynamics of the regional atmospheric system in a fully non-linear and systematic way. The analysis is based on a number of targeted sensitivity experiments using the numerical weather prediction model ICON (Icosahedral Nonhydrostatic), sys- tematically changing the optical thickness of the model clouds. This allows us to clarify the impact of the inter-model spread in cloudiness found in Hannak et al. (2017) on the overall monsoon development in both parameterized and explicit regimes of convec- tion. Although aerosols are not directly modeled in our experiments, the effects found for imposed changes of cloud optical thickness also help to understand variations of the natural system brought about by aerosol effects on cloud properties and radiation, which in a similar way control the amount of shortwave radiation reaching the surface or interact with clouds through modifications in the diurnal cycle of the PBL (e.g. Deetz et al., 2018a).

This article is structured as follows: in Sect. 2 the data and methods are introduced together with a description of the ICON model and the experimental design. The results of the sensitivity experiments are presented in Sect. 3, where we first consider the thermodynamic and dynamic effects on the southern West African region, where we modify clouds. Later we expand the analysis to the greater WAM region including the Sahel. The results are further discussed and summarized in the concluding Sect. 4.

2 Data and methods

This section first details the observational data (ground- and space-based) used as a reference for our modeling experiments (Sect. 2.1), followed by a general description of the ICON model and the design of the sensitivity experiments (Sect. 2.2). The analysis will concentrate on July 2006 and spatially on the DACCIWA study region ($5° - 10° N, 8° W - 8° E$, visualized in Fig. 1), as used in several related papers (e.g. Hannak et al., 2017; Hill et al., 2018). July 2006 was characterised by a relatively late monsoon onset as documented for example in Janicot et al. (2008).

2.1 Observational data

2.1.1 Precipitation

Precipitation information from two different sources are considered in this study. The first is the Tropical Rainfall Measuring Mission (TRMM) 3B42 version 7 dataset. TRMM is a joint mission of the National Aeronautics and Space Administration and the Japan Aerospace Exploration Agency covering the tropical and subtropical regions of the earth during 1997–2015. This dataset is created with the TRMM Multisatellite Precipitation Analysis method (Huffman et al., 2007) combining the TRMM precipitation radar with measurements from microwave and infrared sensors on several low earth orbiting and geostationary satellites, and is calibrated with rain gauge data on a monthly basis. The rainfall data used in this study were aggregated from 3-hourly measurements on a $0.25° \times 0.25°$ grid.

In addition to TRMM, rainfall from the Global Precipitation Climatology Project (GPCP) was used. GPCP combines several sources of rainfall measurements into one global dataset with a high data density and accuracy. It was established by the World Climate Research Programme to quantify the distribution of precipitation around the globe on climatological time scales (Adler, 2003). In GPCP, ground-based rain gauge measurements as well as satellite-based precipitation estimates are combined to give a merged product. The rain gauge measurements stem from the Global Precipitation Climatology Centre monitoring product of the German Weather Service (DWD). The satellite data consist of infrared and microwave radiance-derived rainfall estimates from geostationary as well as polar orbiting satellites. We used daily data in $1.0° \times 1.0°$ horizontal resolution.

2.1.2 Radiation

SSI measurements stem from the climate data record SARAH (Surface Solar Radiation Data Set Heliosat) version 2. It was created by the Satellite Application Facility on Climate Monitoring (CM SAF) based on Meteosat Visible and Infrared

Imager (MVIRI) and Spinning Enhanced Visible and InfraRed Imager (SEVIRI) measurements on the geostationary Meteosat satellites (Müller et al., 2015). From MVIRI, the broadband visible channel and from SEVIRI the channels 0.6 and 0.8 μm are used. SARAH was produced using a retrieval system based on the Heliosat method and an efficient clear-sky surface solar radiation transfer model (Mueller et al., 2009; Posselt et al., 2012). For this study we use the monthly mean products of the dataset with a horizontal resolution of $0.05° \times 0.05°$. In addition, we employ the much-coarser EBAF-Surface Ed4.0 dataset (Energy Balanced And Filled) containing monthly averaged SSI fields with a horizontal resolution of $1° \times 1°$. This product is based on the CERES (Clouds and the Earth's Radiant Energy System) algorithm (Loeb et al., 2009; Young et al., 1998), which uses information from the CERES shortwave broadband radiometers but also from instruments on geostationary satellites to account for the diurnal variability in the data. Several CERES instruments are mounted on polar orbiting satellites such as TRMM, Terra, Aqua and NPP (Suomi National Polar-orbiting Partnership). To derive the radiative fluxes at the surface, cloud imager data for scene classification, cloud physical properties, temperature, water vapor, ozone and aerosol data as well as a broadband radiative transfer model are needed.

The satellite-derived SSI fields are complemented with a small set of surface measurements. Unfortunately, there are very few ground-based measurements of SSI available in the DACCIWA study region during July 2006. South of $10°N$, only the stations Lamto (Ivory Coast, $6.22°N, 5.03°W$), Cotonou and Parakou (both Benin, at $6.35°N, 2.43°E$ and $9.33°N, 2.62°E$, respectively) delivered gap-free measurements from standard instruments, i.e. a Gunn-Belani radiometer (Lamto) and CNR1 radiometers from Kipp & Zonen (Parakou and Cotonou).

For OSR at TOA, monthly mean averages from the dataset GERB/SEVIRI ed. 2.0 from CM SAF (Clerbaux et al., 2017) were used. GERB is the geostationary earth radiation budget instrument onboard Meteosat Second Generation satellites (Harries et al., 2005). This broadband radiometer is designed to measure the earth's total emitted longwave and solar reflected radiances with high temporal resolution (5 min) and 50 km grid-spacing. It is available as TOA reflected shortwave and TOA emitted thermal fluxes. In the present study, we consider only the shortwave flux. For this dataset, SEVIRI measurements are employed to refine GERB's original spatial resolution to a $0.1° \times 0.1°$ grid. In addition, the $1° \times 1°$ monthly EBAF-TOA Ed4.0 dataset for shortwave radiation is used that has been derived using the same CERES algorithm as for the surface.

2.2 Modeling experiments

2.2.1 General model description

The highly scalable ICON model (Zängl et al., 2014) was recently developed by the Max Planck Institute for Meteorology and the DWD, and became DWD's new operational global NWP in January 2015. ICON's horizontal Arakawa C type grid is based on triangles, which cover the globe with approximately equal area everywhere, and allow easy nesting. The vertical coordinate is height-based and terrain-following in the lower levels but smoothed in the upper troposphere via the application of a SLEVE (smooth level vertical) coordinate (Leuenberger et al., 2010). For the dynamical core the continuity equation is formulated in the flux form with density as the prognostic variable, enabling exact local mass conservation. The equations are solved non-hydrostatically and the time integration is performed with a two-time-level predictor-corrector scheme. Apart from the sound

wave propagation, this scheme is fully explicit. The fast physics packages are inherited from the Consortium for Small-scale Modelling (COSMO) model (Doms and Schättler, 2004) but are partly reformulated for ICON. The cloud microphysics scheme is the COSMO-EU five-category prognostic scheme (Doms and Schättler, 2004; Seifert, 2008) with the extension of ice sedimentation. The turbulence scheme by Raschendorfer (2001) solves the prognostic equation for turbulent kinetic energy (TKE) and for the land-surface interaction TERRA (Heise, 2006) is used in an updated version. The slow physics parametrizations correspond to those from the Integrated Forecasting System (IFS) of the European Centre for Medium-Range Weather Forecasts (ECMWF): the Bechtold et al. (2008) convection scheme, the Lott and Miller (1997) subgrid-scale orography scheme and the Orr et al. (2010) non-orographic gravity-wave drag scheme. Radiative transfer is solved with the Rapid Radiation Transfer Model (RRTM, Mlawer et al., 1997), where a Green's function approach is applied for solar bands with approximated diffuse radiation (Barker et al., 2002).

Currently ICON is only configured as a global model but its high flexibility in terms of one- and two-way nesting allows a regional focus without any undesirable boundary effects sometimes observed for traditional limited-area models. It performed well compared to ERA Interim (ERA-I hereafter) in several test cases we ran for DACCIWA. The comaprison can be found in the supplementary material. The simulation period was not so much limited by computational cost but by the large amount of output, since many different state variables had to be saved for the analysis.

All simulations in this paper were initialized with ERA-I, ECMWF's global atmospheric reanalysis (Dee et al., 2011), and do not use data assimilation. ERA-I is created by assimilating all available measurements into a single forecast model environment, resulting in a multivariate, spatially complete and coherent record of the global atmospheric state. ERA-I data are used in the highest possible horizontal resolution of about 80 km and with 60 vertical levels up to 0.1 hPa. Typically ERA-I contains most observations at 12 and 00 UTC. Initializing ICON runs at 00 UTC would mean starting the runs during the development phase of the low-level clouds and therefore the runs were initialized at 12 UTC.

2.2.2 Design of experiments

To assess the impact of variations in cloudiness in the ICON model, a series of experiments was designed. In these, the original cloud liquid water content q_c in the DACCIWA study region and below 700 hPa (see Fig. 1) is manipulated immediately before the call of the radiation scheme by multiplying it with an opacity factor f_{op} to mimic an increase or decrease of the low clouds' optical thickness. After that, q_c is set back to the original value and the model is allowed to run freely until the next call of the radiation routine. In this way it is ensured that only the radiation can impact on the dynamics and thermodynamics, creating changes in temperature T, relative humidity RH and winds etc., which in turn can influence the development of clouds itself. f_{op} is varied from 0.1 to 10, where $f_{op} = 1$ corresponds to the control experiment. The low values are at the extreme end of cloud underrepresentation found in Hannak et al. (2017), while $f_{op} = 10$ should be regarded as a somewhat unrealistic sensitivity test.

Two sets of experiments were performed with ICON:

1. PARAM: For this set, ICON was run in the current operational global setting with a horizontal grid spacing of 13.2 km and 91 vertical levels. Integration time is five days. f_{op} is varied in eight steps from 0.1 to 10.0 to systematically analyze the effect of low-level clouds. Due to the relatively high computational costs, runs are restricted to July 2006 and only started every 4^{th} day in order to have one day of overlap between the simulations. All in all 8×8 5-day simulations were performed for this set.

2. EXPL: The overall setting is identical to PARAM, but another nest was added to achieve 6.6 km horizontal resolution, which allowed switching off the convection scheme. The nest has a circular domain centered on 0° E and 13° N with a radius of 30° such that it is large enough to avoid undesirable effects near the nest's boundary. In order to keep the amount of data manageable, only two f_{op} values were run: 0.1 and 1.0. This will show whether the sensitivities found for PARAM depend on the convection scheme, as demonstrated for example for the larger WAM circulation by Marsham et al. (2013). One may argue that 6.6 km is still too coarse for explicit convection, but Marsham et al. (2013) showed that for West Africa explicit convection even at a grid-spacing of 12 km improves the diurnal cycle of the PBL and convection.

The same study differentiated between the effect of parametrization and the effect of horizontal resolution by comparing experiments with 12 km grid-spacing and both parametrized and explicit convection as well as explicit convection at 4 km. It was found that the dominating factor is the convective parametrization, which substantially alters the dynamics of the monsoon system, while the influence of the horizontal grid-spacing is mainly of quantitative nature. Building on these results, we will concentrate on differences between parametrized and explicit convection and pay less attention to resolution effects.

3 Results

In this section we will discuss the outcome of the control and sensitivity experiments. The analysis will be broken down in four parts. The first section (Sect. 3.1) will concentrate on a general model evaluation over West Africa comparing ICON PARAM and EXPL with observations. Sect. 3.2 analyses diurnal-mean responses over the DACCIWA study region considering the full range of f_{op}. Sect. 3.3 discusses the impact of cloud modification on the diurnal cycle covering a wide range of parameters including precipitation, clouds, temperature and humidity for southern West Africa, while the following Sect. 3.4 will analyze impacts on the wider WAM region. Sects. 3.2–3.4 also contain a systematic comparison between the PARAM and EXPL experiments. A geographical map of southern West Africa indicating the study region and locations mentioned in the analysis is shown in Fig. 1.

3.1 Model evaluation

Here a characterization of the meteorological conditions in southern West Africa for the wet monsoon month July 2006 is given, concentrating on precipitation and radiation. Comparison of ICON runs with observations will reveal the applicability of the ICON model for the following experiments and the sensitivity to convective parametrization.

Figure 1. Map of southern West Africa indicating the geographical locations referenced in the text. Low-level clouds were modified within the pink square.

Figure 2 shows July 2006 averaged daily precipitation for ICON EXPL, ICON PARAM, TRMM and GPCP together with the respective averages over the DACCIWA region as numbers. TRMM and GPCP are shown in their native resolutions, while ICON EXPL and ICON PARAM are interpolated to grids with $0.0625° \times 0.0625°$ and $0.125° \times 0.125°$ spacings, respectively. The averages were created from the final four days of the five day simulations. All four datasets have marked local maxima over the Niger Delta region in Nigeria and the adjacent Adamawa Highlands as well as along the coast of Guinea, Sierra Leone and Liberia and adjacent Guinea Highlands. Within our main region of interest, there are substantial differences with respect to the position of the main rainband. The two observational datasets, TRMM and GPCP, consistently show a well defined zonal rainband stretching across the Sahel with substantially drier conditions over southern West Africa and the adjacent Atlantic Ocean (Figs. 2c and d). There is, however, some conspicuous disagreement between the two in coastal areas, where satellite retrievals are complicated by the sharp change in surface properties, illustrating the overall observational uncertainty, which is also related to the (relatively sparse) ground-based network. ICON EXPL produces a much wetter, northward shifted main rainband compared to ICON PARAM with a lot of fine structure related to the high spatial resolution (Fig. 2a). In stark contrast, ICON PARAM struggles to represent the shift of rainfall inland resulting in substantially lower amounts in the Sahel (Fig. 2b). Within the DACCIWA box, area-averaged rainfall agrees within less than 10% between the observational datasets. Despite the overall dry bias of ICON PARAM, agreement with observations in the DACCIWA box is satisfactory, while ICON EXPL underestimates rainfall by about 30% (3.3 $\mathrm{mm\ day^{-1}}$ vs. 4.7 $\mathrm{mm\ day^{-1}}$ for TRMM and GPCP combined). At least some of the patterns within the DACCIWA box (e.g. slightly moister northwestern corner over Ivory Coast, drier Lake Volta region and a local maximum over the Atakora chain) are consistent between all four datasets. The small middle panels in Fig. 2 show the rainfall dependent on latitude but averaged over $8°W - 8°E$, as it is further analysed in section 3.4.1. The rainfall maxima over

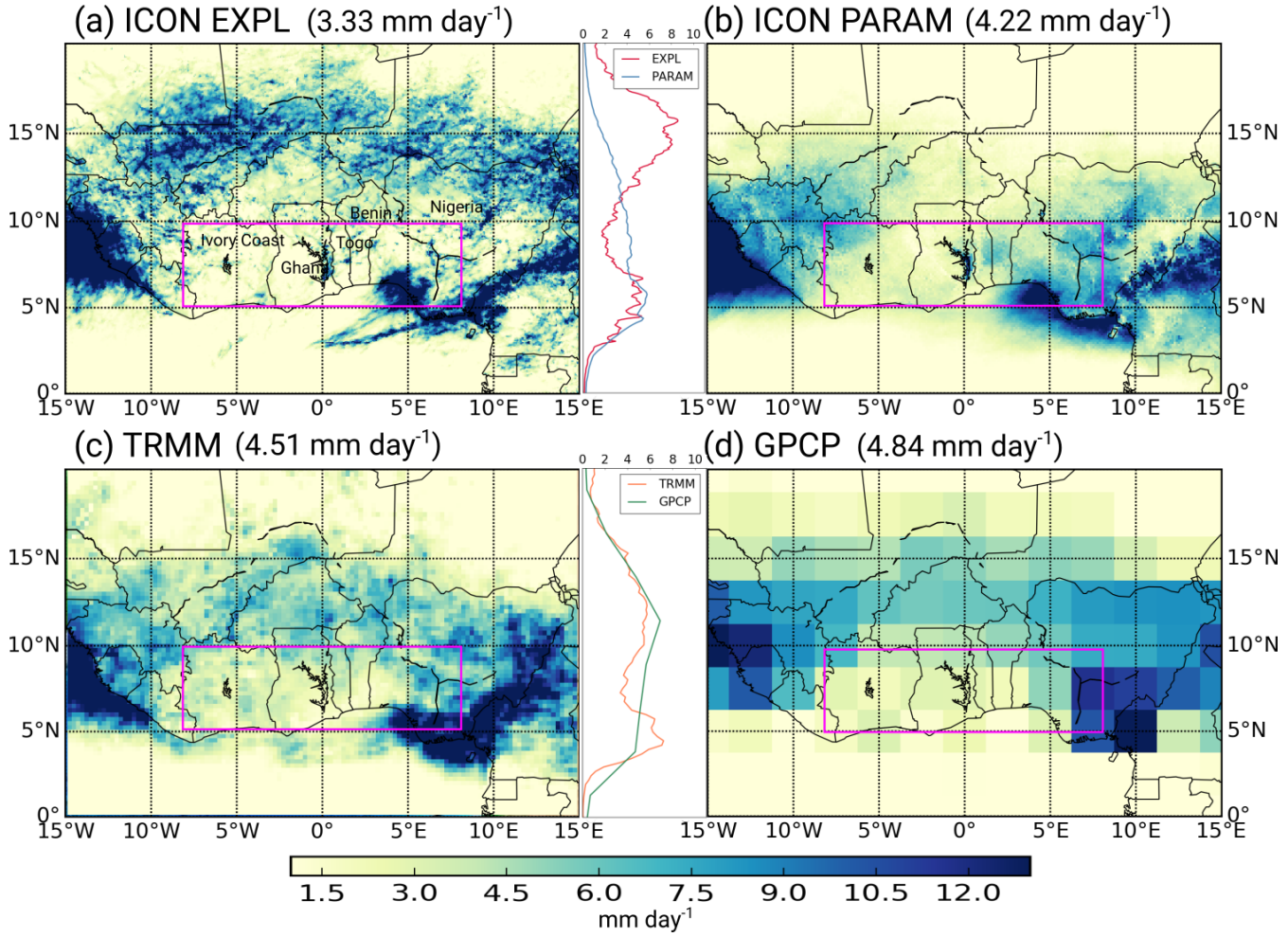

Figure 2. Mean daily rainfall for July 2006 over the larger West African domain for (a) ICON EXPL, (b) ICON PARAM as well as the observational datasets (c) TRMM and (d) GPCP with averages over the DACCIWA box (marked with pink square) on top of each panel. The two small graphs between the panels contain the rainfall dependent on latitude, averaged over $8°W - 8°E$.

the Niger Delta region and along the coast of Guinea, Sierra Leone and Liberia are not captured in this average, which explains the rather small values between 7-10°N.

This comparison reveals an enormous sensitivity of the WAM to convective parametrization. In agreement with Marsham et al. (2013) explicit convection creates substantially more rainfall but the northward shift we observe for ICON was not found for the Unified Model used in that study. Ultimately, the low agreement between the two ICON simulations and with observations hampers drawing rigorous quantitative conclusions from our sensitivity experiments and forces us to analyse all subsequent aspects separately for PARAM and EXPL. However, the errors in latitudinal position and intensity of the Sahelian rainband

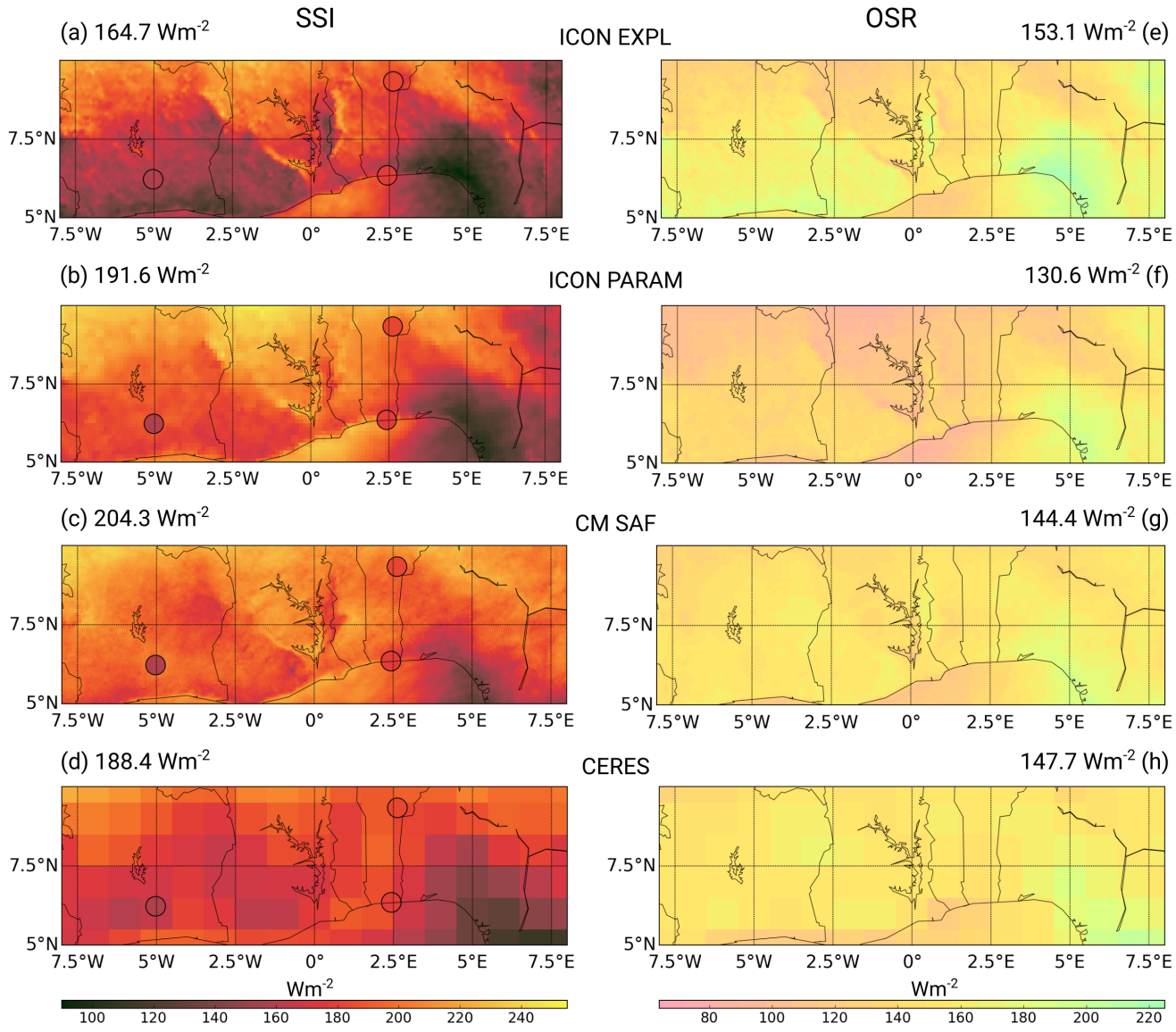

Figure 3. Mean July 2006 SSI over the DACCIWA box from (a) ICON EXPL and (b) ICON PARAM as well as the satellite-derived datasets (c) CM SAF and (d) CERES plus station data as filled circles. Corresponding OSR fields are given in (e)–(h). Area averages are provided on top of each panel.

we find here are commonplace in intercomparison studies for climate models (Mohino et al., 2011; Roehrig et al., 2013) and allow interfering whether the sensitivities we find are robust against these differing model basic states.

Fig. 3 shows comparisons between ICON EXPL and PARAM with the observational datasets CM SAF and CERES for SSI (left) and OSR (right), again in their native resolution with DACCIWA-box averages provided as numbers. Additionally, surface radiation measurements from the ground stations in Lamto, Cotonou and Parakou are included for comparison. The depiction is limited here to the DACCIWA box, as this is where our main interest in clouds lies. SSI depends on how much sunlight is absorbed or reflected on its way through the atmosphere, mostly by clouds but also by aerosols. This is clearly illustrated in the high-resolution datasets, ICON and CM SAF, where the relatively cloud-free western Bight of Benin and Lake Volta area show local maxima (Figs. 3a–c). All datasets reveal a general tendency for lowest SSI in the inland "stratus belt" around 7°N and an increase towards the less cloudy Sahel in the north. Minima are usually found over southwestern Nigeria with values dropping to below 120 W m^{-2}. In addition to many smaller differences in pattern, there are quite considerable deviations in absolute values between the four datasets.

ICON EXPL shows the lowest SSI values with an area average of 164.7 W m^{-2} (Fig. 3a), much lower than PARAM with 191.6 W m^{-2} (Fig. 3b). We will see later in this paper that there likely is a direct connection between this and the much lower rainfall found in EXPL through an increase in vertical stability due to less sunlight reaching the ground. Evaluating this with observations is a challenge due to the many assumptions made in satellite-derived SSI and the few surface observations. CM SAF shows an overall similar pattern as the two ICON simulations but with systematically higher values inland and an area average of 204.3 W m^{-2} (Fig. 3c). This is clearly at odds with the ground stations and is likely due to the method of determining the range of minimum and maximum irradiance for the applied self-calibration. As cloudy pixels appear brighter than cloud-free ones for SEVIRI, the surface albedo is estimated from the lowest irradiance measurement found per pixel in a given time period. In SWA, however, it is often difficult to find cloud-free scenes, leading to an overestimation of surface albedo (see also discussion of this problem in Hannak et al., 2017). Therefore it suggests an unrealistically bright surface (see also discussion of this problem in Hannak et al., 2017). In contrast, CERES does not seem to suffer from this problem due to a different retrieval strategy (Fig. 3d). The box-averaged SSI is 188.4 W m^{-2} and therefore very close to the ICON PARAM value, although with much less fine structure. Overall this analysis demonstrates a significant observational uncertainty and suggests an overestimation of clouds in ICON EXPL leadin to low average SSI, while ICON PARAM fields are more consistent with observations in this regard.

The right panels in Fig. 3 show corresponding fields of OSR. Given that this quantity can be measured directly from satellite, it is no surprise that the agreement between the two observational datasets is much closer, apart from, of course, the obvious differences in resolution (Figs. 3g and h). Nevertheless, even here there is a non-negligible observational uncertainty with the area averages differing by 3.3 W m^{-2}, corresponding to 2%. There are many structural similarities to SSI (left panels of Fig. 3) but with the opposite sign, indicating that clouds suppress SSI but increase OSR due to their high reflectivity. Consistently, ICON EXPL shows the highest area-averaged OSR of 153.1 W m^{-2} (Fig. 3e). In contrast, ICON PARAM produces much lower values of only 130.6 W m^{-2} (Fig. 3f). Given an SSI similar to CERES, this suggests an overestimation of scattering on cloud droplets, i.e. biases in the amounts of cloud water or ice or their size distributions. This comparison reveals that the substantial differences between PARAM and EXPL found for precipitation also hold for cloud radiative effects and that the dissatisfying agreement with observations somewhat limits the quantitative interpretation of our sensitivity experiments.

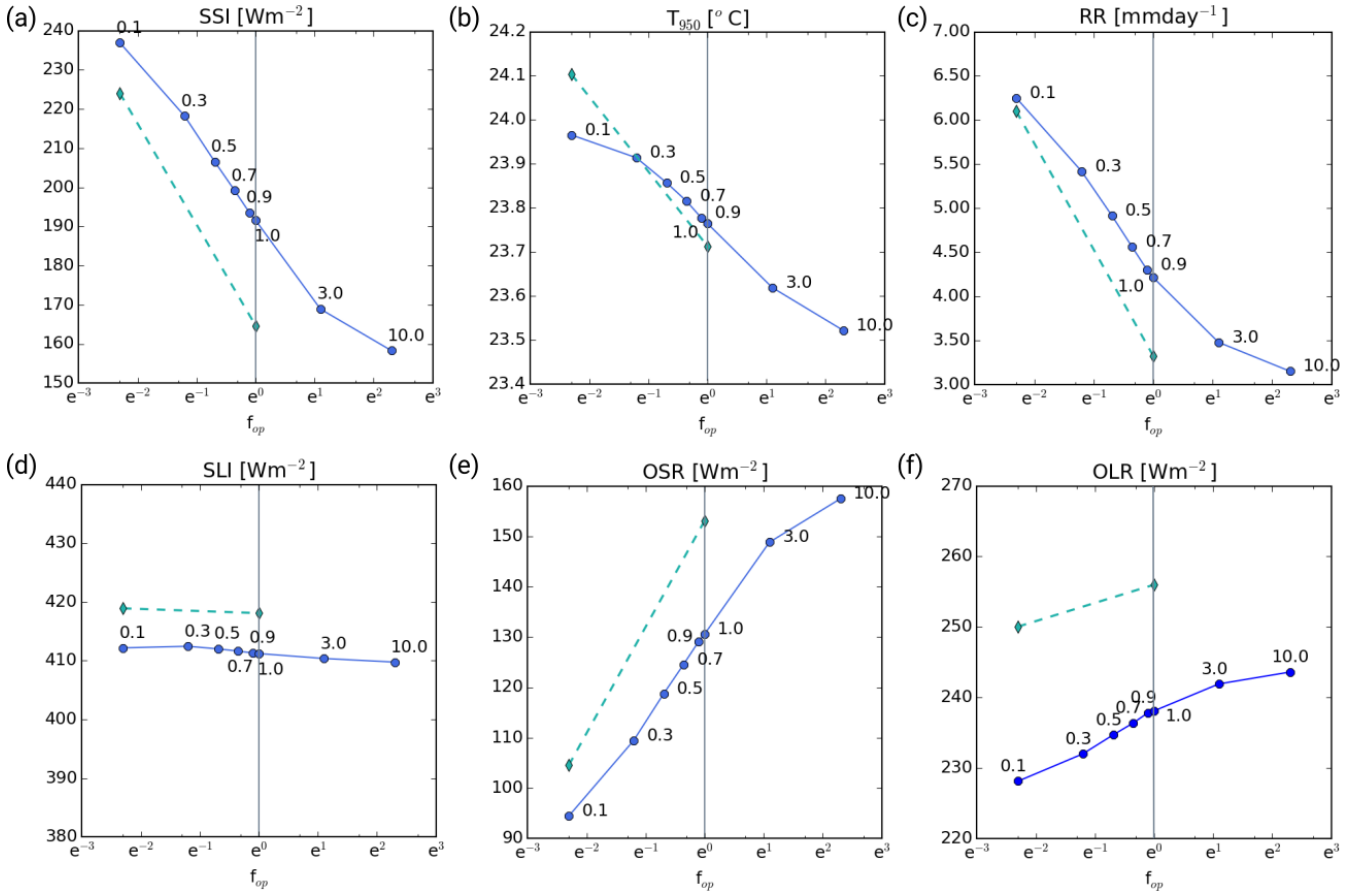

Figure 4. Averages over July 2006 and the DACCIWA box of SSI (a), T at 950 hPa (b), precipitation (RR) (c), SLI (d), OSR (e) and OLR (f) depending on the opacity factor f_{op} plotted with an exponential scale. ICON PARAM is depicted with solid blue lines, while the dashed cyan lines denote ICON EXPL (see Sect. 2.2.2). The thin grey line marks the position of the control run $f_{op} = 1.0$.

3.2 Dependence of diurnal mean fields on f_{op}

In this section, first results for the modifications of f_{op} in ICON (see Sect. 2.2.2) will be presented for PARAM and EXPL. Parameters considered for this investigation are precipitation, SSI and OSR as in Sect. 3.1 and additionally temperature at 950 hPa T_{950}, outgoing longwave radiation (OLR) and surface longwave irradiance (SLI), all averaged over the DACCIWA box as in Fig. 3. The questions to be addressed in this section are: (a) How is the sensitivity of the considered parameters to f_{op}? (b) How do the fully nonlinear processes represented in ICON differ from the purely radiative transfer computations by Hill et al. (2018)? (c) To what extent does the signal depend on the use of a convective parametrization (comparing PARAM with EXPL)?

In PARAM, SSI decreases largely logarithmically with increasing optical thickness (Fig. 4a), ranging from 158.2 W m^{-2} to 236.9 W m^{-2}. Only at the highest f_{op} of 10 is there a clear indication for a certain "saturation" of the signal. Given this

behavior in SSI, it is to be expected that T_{950} also decreases with f_{op} (Fig. 4b). The small range, however, of less than $0.5°C$ (23.5–24.0$°C$) suggests that some of the additional radiative heating of the surface is balanced by transports into the atmosphere, i.e. either a deeper PBL or convection. This is consistent with the flatter curve at the lowest f_{op} values. Figure 4c demonstrates that the effects on precipitation are in fact enormous, leading to a doubling in daily precipitation from 3.2 mm for $f_{op} = 10$ to 6.3 mm for the optically thinnest clouds with $f_{op} = 0.1$. The shape of the curve is very similar to that of SSI (Fig. 4a), indicating a strong control of radiation on convective initiation.

With respect to the other components of the radiative budget, Fig. 4d shows that SLI is hardly affected varying between 412.5 and 409.8 W m^{-2} only, which corresponds to less than 0.7%. This low sensitivity is the result from small variations in low-level temperature (Fig. 4b) and an overall very moist atmosphere that traps longwave radiation , almost irrespective of low-level clouds. At TOA, both longwave and shortwave outgoing radiation increase with increasing f_{op} (Figs. 4e and f). Again, the variation in shortwave radiation dominates over that in the longwave (from 94.4 to 157.5 W m^{-2} and from 228.2 to 243.6 W m^{-2}, respectively). The increase in OSR is consistent with the increased reflection from low-level clouds, as already discussed in the context of Fig. 3. The difference in SSI and OSR signals shows that extinction increases with increasing f_{op}. As will be seen later, this extinction is caused by scattering on cloud droplets and absorption of water vapour. The increase in OLR is consistent with the decrease in precipitation (Fig. 4c) associated with less deep convective clouds.

The simple linear model used by Hill et al. (2018) allows a rough estimate of how much of the change in the ICON radiative fluxes (Fig. 4) is due to direct radiative effects and how much is due to the dynamical response of the system. Ignoring all clouds below 680 hPa, their radiative transfer calculations for June–September 2006–2010 yield the following signals: increases of 35 W m^{-2} in SSI and of 2 W m^{-2} in OLR as well as decreases of 25 W m^{-2} in OSR and of 11 W m^{-2} in SLI. Comparing these values with differences between f_{op} of 1.0 and 0.1 in Fig. 4 shows that the ICON PARAM-generated responses in shortwave radiation for July 2006 have a larger amplitude. Given the reasonable agreement with CERES in SSI (Fig. 3) and the slightly shallower layer of cloud modification (below 700 hPa vs. below 680 hPa), this is a surprising result. The most plausible explanation is that the relatively dry July 2006 had overall less mid- and high-level clouds than the June–September 2006–2010 average used inHill et al., leading to a relatively larger effect of low-level cloudiness (consistent with Fig. 9 in Hill et al., 2018). This makes it hard to distinguish the purely radiative signal from the fully nonlinear dynamical response of the atmosphere. The latter is more distinguishable in the longwave component. The increase in deep convection with optically thinner low clouds in ICON PARAM leads to a decrease in OLR in the model on the order of 10 W m^{-2}, while the radiative transfer calculations by Hill et al. show even a small increase. In contrast, for SLI the purely radiative effect is a marked decrease, but ICON-PARAM shows almost constant SLI, likely due to combined dynamical effects of the increase in low-level temperature, deep convective clouds and column moisture (see Fig. 12).

Finally, the differences between PARAM and EXPL in Fig. 4 illustrate the sensitivity of the response to horizontal resolution and the use of convective parametrization. The overall behavior of EXPL (dashed lines in Fig. 4, f_{op} values of 1.0 and 0.1 only) is comparable but there are deviations in terms of basic state and sensitivity. As already discussed, EXPL has more clouds, leading to lower SSI and higher OSR (both on the order of about 20 W m^{-2}; Figs. 4a and e). Interestingly, the low-level temperature is almost identical for $f_{op} = 1.0$ but slightly warmer in EXPL for $f_{op} = 0.1$ (Fig. 4b), indicating subtle

differences in the surface energy budget. Despite the warmer temperatures, precipitation is always lower than in PARAM (Fig. 4c), suggesting that convection is less easily triggered in EXPL (daily sums are 3.3 and 6.1 mmh^{-1} for $f_{op} = 1.0$ and $f_{op} = 0.1$, respectively). This could be an explanation for the overall higher sensitivity in EXPL, making the simulation even more dependent on modifications of solar radiation reaching the ground. With respect to longwave components (Figs. 4d and f) EXPL shows higher SLI and higher OLR (about 8 and 20 $\mathrm{W\ m^{-2}}$, respectively). The former is consistent with more low-level clouds for $f_{op} = 1.0$ and warmer low-level temperatures for $f_{op} = 0.1$. The latter mirrors the reduced ice content of EXPL compared to PARAM in the upper levels of the troposphere (see right panels of Fig. 6), which facilitates the escape of longwave radiation to space and therefore enhances OLR.

3.3 Impact on the diurnal cycle

In this section we will continue analyzing the effect of modifying the optical thickness of low clouds, but here with a focus on the diurnal cycle. The analysis begins with impacts on precipitation and clouds followed by an investigation of the vertical structure of the signal.

3.3.1 Precipitation and clouds

For precipitation, PARAM generally shows a distinct maximum at 15 UTC (corresponding to local time in our study region) and lowest rainfall in the second half of the night (Fig. 5). Consistent with Fig. 4c, a decrease in f_{op} leads to a monotonic and smooth increase in precipitation at all times of day, apart from the early morning hours, when the effect is weak. At the time of maximum precipitation, the rainfall from experiment $f_{op} = 0.1$ is 2.5 times larger than that for $f_{op} = 10.0$. The morning onset of rainfall is earlier for low f_{op}, as the buildup of instability due to incoming solar radiation occurs faster after sunrise. EXPL shows some significant differences (blue lines in Fig. 5). The diurnal peak is shifted to 18 UTC, as it takes more time to trigger convection without a parametrization (Marsham et al., 2013). This corresponds much better to the typical timing of precipitation observed in this area (Kalthoff et al., 2018) and to the TRMM observations included in Fig. 5, despite the overall large bias already discussed (Fig. 2). The onset of precipitation is not strongly affected by f_{op} in EXPL, but the cessation is, with convection persisting much longer into the night for the optically thinnest low-level clouds, suggesting a much higher degree of organization. The latter is reflected in a larger variance of q_v throughout the lower and mid-troposphere in EXPL than in PARAM (not shown). We have no explanation for the kinks in the curves around 12 UTC in EXPL and therefore attribute those to insufficient sampling. In terms of the diurnal maxima, values for EXPL are systematically lower with 0.17 and 0.47 $\mathrm{mm\ h^{-1}}$ for $f_{op} = 1.0$ and $f_{op} = 0.1$, respectively, compared to 0.32 and 0.5 $\mathrm{mm\ h^{-1}}$ for PARAM.

Figure 6 shows the diurnal cycle in the vertical structure of cloud cover CLC, cloud water content q_c and cloud ice content q_i for PARAM and EXPL and for f_{op} values of 0.1 and 1.0. PARAM shows a clear three-layer cloud structure at all times of day as documented for other tropical regions (e.g. Johnson et al., 1999). Low-level clouds are mostly confined to below 750 hPa with a relatively minor mid-level cloud layer around 500–600 hPa. While the former contain significant amounts of q_c (middle column of Fig. 6), the midlevel clouds also contain some cloud ice (right column of Fig. 6). In addition, a substantial high-level cloud cover between 400 and 100 hPa containing significant amounts of cloud ice is simulated in PARAM. In particular the

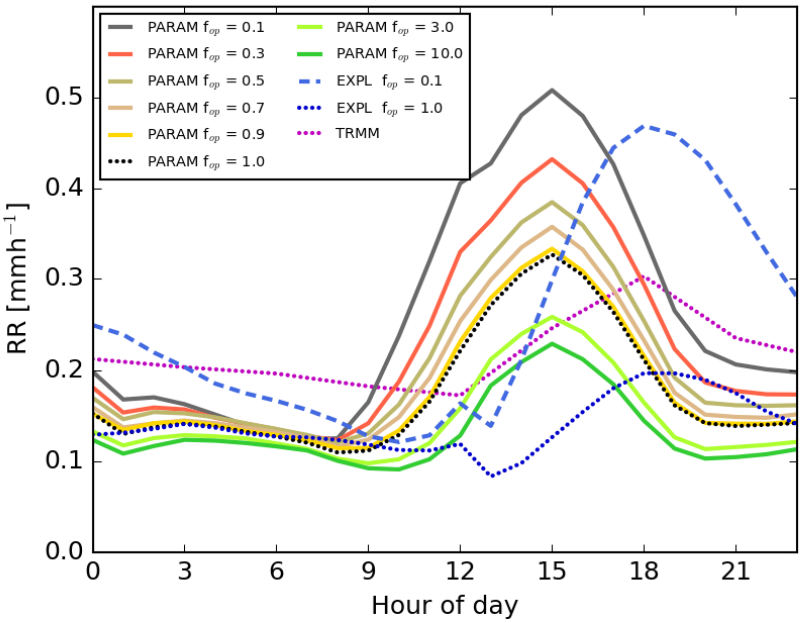

Figure 5. Diurnal cycle of precipitation averaged over the DACCIWA box and for July 2006. Solid lines show PARAM simulations for varying f_{op}, and the dashed line shows the EXPL simulation for $f_{op} = 0.1$. Dotted lines denote PARAM and EXPL simulations with $f_{op} = 1.0$, and additionally TRMM observations.

low and high clouds show a distinct diurnal cycle. At 00 UTC the low-level cloud deck is beginning to form, reaching a sharp peak around 950 hPa at 06 UTC accompanied by a corresponding increase in q_c (Figs. 6a and b). At midday (Fig. 6c), radiative heating lifts and dissolves the low-level cloud deck shifting the maximum in CLC and q_c to 850 hPa (Fig. 6c). Finally by 18 UTC (Fig. 6d) daytime heating and mixing have reduced CLC and q_c to create a diurnal minimum. This general diurnal behavior in low-level cloudiness in PARAM resembles that found in ECMWF analysis data (see Hannak et al., 2017). Midlevel clouds do not show pronounced diurnal variations but also have a minimum in CLC and q_c at 18 UTC, possibly suggesting similar mechanisms as for the low clouds. High-level CLC and q_i are lowest at 12 UTC and highest at 00 UTC, when they reach, respectively, more than 30% and almost 0.008 $\mathrm{g\ kg^{-1}}$. This indicates a relationship of high-level clouds with the diurnal cycle of convection (Fig. 5) leading to an increase in the second half of the day.

Reducing the optical thickness of low clouds in PARAM ($f_{op} = 0.1$; dashed green lines in Fig. 6) has hardly any impact on low-level CLC during nighttime but leads to a small decrease at 12 UTC and an even lesser decrease at 18 UTC, possibly due to a deeper and/or drier PBL. Surprisingly, however, q_c is decreased by on the order of 0.01 $\mathrm{g\ kg^{-1}}$ at all times and most strongly so at 00 UTC, indicating that for $f_{op} = 0.1$ a similar cover of clouds is achieved with less liquid water. This aspect will be further discussed in the following subsection. For high clouds in contrast, both CLC and q_i increase markedly for all times with absolute increases on the order of 7% and 0.005 $\mathrm{g\ kg^{-1}}$ at the peak of the profile at about 250 hPa. This is

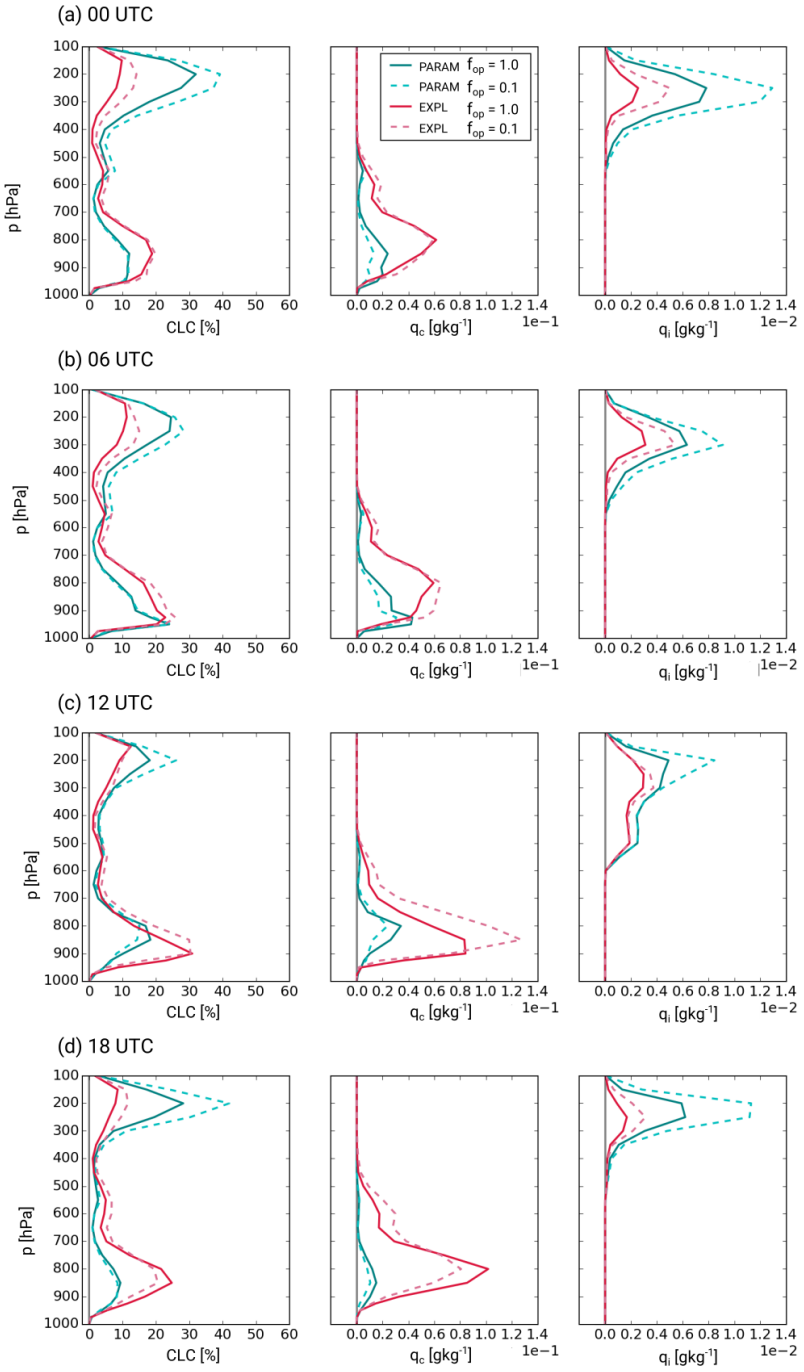

Figure 6. July 2006 mean profiles of CLC, q_c and q_i averaged over the DACCIWA box for experiments PARAM (green) and EXPL (red) and varying f_{op} according to the legend at the top: (a) 00 UTC, (b) 06 UTC, (c) 12 UTC and (d) 18 UTC.

likely a reflection of the increased daytime convection in the sensitivity experiment, leading to more precipitation (Fig. 5) and generating substantially more cirrus. This also suggests that part of the effect of more solar radiation reaching the surface through the optically thinned low clouds is compensated by an increase in high clouds. The comparison with the radiative transfer results by Hill et al. (2018) in the previous section, however, suggests that this is a relatively small effect overall.

Comparing the results for PARAM with those for EXPL reveals some substantial differences. Low clouds are more abundant in EXPL at all times, as already suspected in Sect. 3.2, contain substantially more liquid water and peak at 12 UTC rather than 06 UTC as in PARAM. q_c can be up to 0.09 gkg^{-1} higher for EXPL. The sensitivity of q_c to f_{op} has a much stronger diurnal cycle with little effect at 00 UTC, a small increase at 06 UTC, a large increase and deepening at 12 UTC followed by a decrease at 18 UTC (middle panels in Fig. 6). Consequently, the signals at 06 and 12 UTC go in the opposite direction in EXPL and in PARAM. This rather unexpected result will be discussed in more detail in the following subsection. In addition there is a small increase in midlevel q_c at all times. In stark contrast, high-level clouds are much reduced relative to PARAM in both amount and q_i at all times with values of up to 0.008 gkg^{-1} lower in EXPL. However, the general sensitivity is similar for high clouds with an increase for $f_{op} = 0.1$ for all times. The magnitude again appears to be related to the diurnal cycle of convection, which is delayed in EXPL relative to PARAM (see Fig. 5). This comparison reveals that in many aspects the variations between EXPL and PARAM are larger than the differences between f_{op} equal to 0.1 and 1.0 for each experiment. To first order, the convective parametrization appears to transport moisture more efficiently out of the low- and mid-levels to deposit it into the convection-fed cirrus layer, as compared to explicit convection. This creates overall less sensitivity to our modifications of low clouds as already discussed in the context of Fig. 4 but also a weaker diurnal cycle in the sensitivities.

3.3.2 Vertical structure

Given the overall higher sensitivities and likely more realistic diurnal cycle in EXPL, we will begin the following discussion of thermodynamic changes with this experiment instead of PARAM. This discussion will help to shed more light into the low-cloud behavior and sensitivities discussed in previous sections. Figure 7 shows DACCIWA box-averaged profiles of differences between the $f_{op} = 0.1$ sensitivity experiment and the $f_{op} = 1.0$ control run for T, specific humidity q_v, RH, turbulent kinetic energy TKE, q_c and horizontal wind speed v_{horiz}. The colored lines show eight different times of day.

With respect to T a relatively complicated vertical profile and diurnal cycle is found. Below 900 hPa, as expected, the reduced optical thickness of low clouds leads to more solar heating during the day and consequently an overall warming peaking at 15 UTC with a slight cooling at 06 UTC (Fig. 7a). Immediately above that, there are indications of enhanced latent heat release within the low-level cloud deck, at least for some times of day when CLC and q_c increase (see Fig. 6) but during the day this effect is not clearly separable from the sensible heat fluxes in the PBL. Above that, around 725 hPa is a shallow layer with a slight cooling, most pronounced during the day and possibly due to radiative effects at the low-level cloud tops. The increases in midlevel cloud and cloud water around 550 hPa (see Fig. 6) also leads to a warming below (latent plus radiative heating) and radiative cooling above, the latter most pronounced at nighttime. Finally, the cirrus layer peaking around 250 hPa also produces such a dipole pattern but with a much smaller diurnal cycle consistent with Fig. 6.

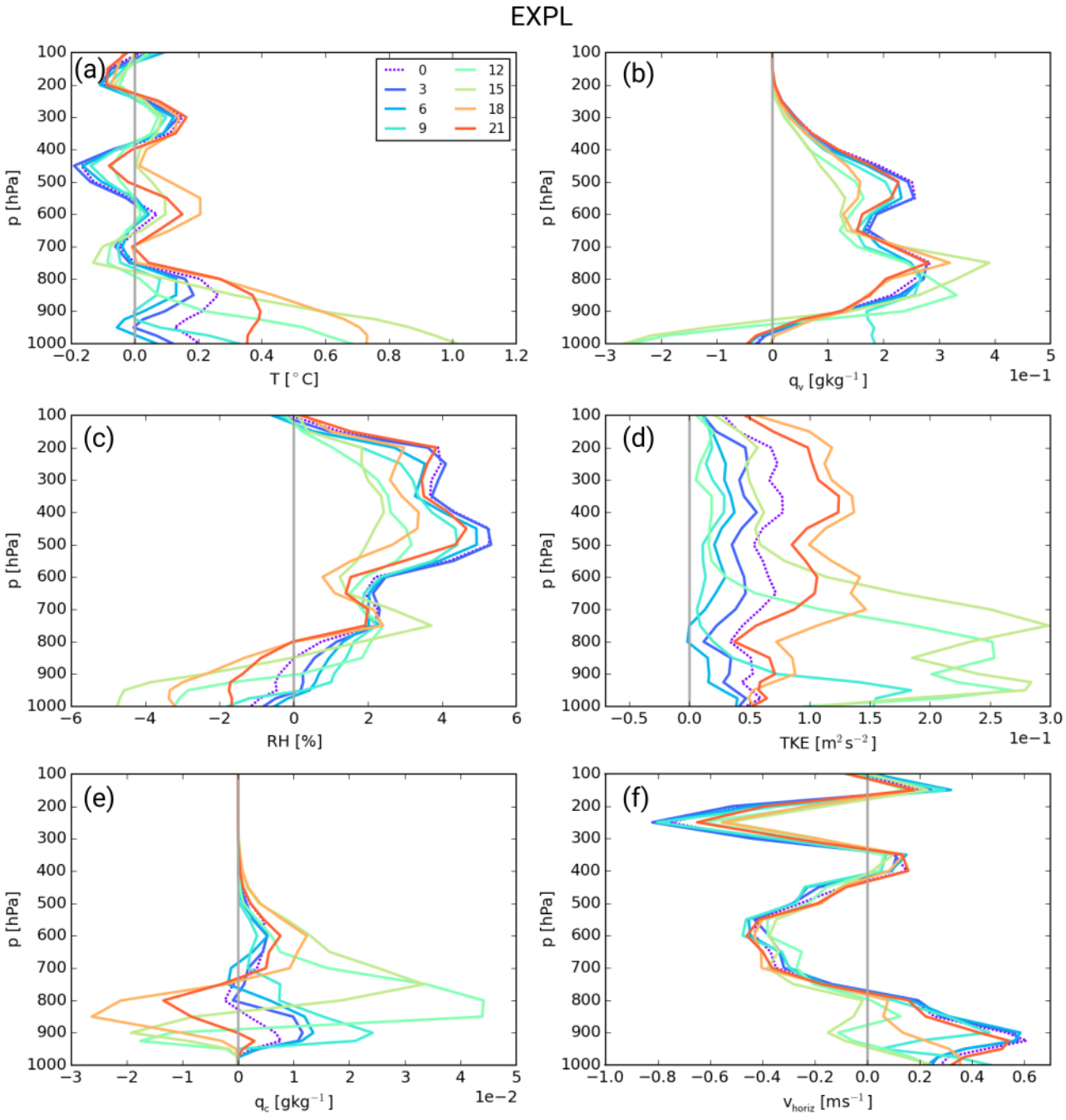

Figure 7. Diurnal cycle (colored lines) of DACCIWA-box and July 2006 averaged profiles of differences $f_{op} = 0.1$ minus $f_{op} = 1.0$ for EXPL showing (a) T, (b) q_v, (c) RH, (d) TKE, (e) q_c and (f) v_{horiz}.

Signals in q_v in contrast are much simpler and show a deep atmospheric moistening at all times (Fig. 7b). The only drying occurs in the lowest few hundred meters at 12 and 15 UTC, when substantial amounts of moisture are pumped into the elevated low-level cloud layer where q_v maximizes. An interesting time is 09 UTC, when q_v is markedly enhanced near the surface. This may be related to an earlier start of the diurnal PBL growth (see discussion on TKE below) or possibly also due to higher evapotranspiration in response to the increased precipitation (see Fig. 5). The second maximum in q_v increase is found in the area of the midlevel cloud layer around 550 hPa. Due to generally low values in the cold upper-troposphere, changes in the cirrus layer are less evident in Fig. 7b. The net increase of column moisture and precipitation (Fig. 5) suggests a substantial increase of moisture convergence into our study region. This will be further discussed in the next subsection. The signal in RH (Fig. 7c) is a combination of the signals in T and q_v. Given the large increases in q_v, RH increases everywhere above 800 hPa at all times of day, with the profile reflecting some of the modulations in the area of the mid- and high-level cloud decks already discussed. Highest RH increases of up to 5.5 % are found in the early morning, at the end of a period with convective moisture transports and radiative cooling. At the very lowest layers, the large increase in T, particularly during the day, leads to a decrease in RH. The level with zero difference descends at night and ascends during daytime. It is lowest at 06 UTC, which facilitates the nocturnal low-level cloud formation for $f_{op} = 0.1$, leading to a slight increase in CLC and q_c (Fig. 6). At 12 UTC RH near the surface is reduced but the higher values above 900 hPa help expanding the cloud deck upwards, while at 18 UTC the drying is so deep that clouds are reduced (cf. Fig. 6).

The discussion so far has illustrated the paramount importance of vertical mixing. To reveal the impact of low-cloud shielding on turbulence, Fig. 7d shows the vertical profile of differences between $f_{op} = 0.1$ and $f_{op} = 1.0$ for TKE, which is increased at all levels and all times. Below 700 hPa turbulence gradually dies down from 18 UTC to 06 UTC. Due to the missing effect of low clouds in $f_{op} = 0.1$, TKE differences increase markedly from 09 UTC to 15 UTC and rise upwards. 12 and 15 UTC show a secondary peak between 850 and 750 hPa, which is probably related to turbulence within the low-level cloud deck. Above 700 hPa, there is rapid increase from low values at 09 and 12 UTC to a maximum at 18 UTC, followed by a gradual decay. This behavior clearly illustrates how deep convection communicates the – at first surface-based – signals into the entire troposphere. Finally, the localized maximum in TKE differences around 900 hPa at night is an indication of a slightly enhanced NLLJ creating turbulence through shear (see Fig. 7f), which in turn helps the cloud formation.

Figure 7e shows the effect of the discussed changes in RH and TKE on q_c, shedding more light into the absolute values already discussed above (solid and dashed red lines in middle panels of Fig. 6). A good starting point to discuss the diurnal cycle of this signal is 18 UTC, when the increase of deep convection is largest (Fig. 5) and creates more clouds above 750 hPa and less in the main low-level cloud deck (Fig. 6d), as the deeper mixing reduces RH (Fig. 7c). At 21 UTC the convective signal weakens and there are some first indications of increased q_c in the nocturnal stratus deck around 925 hPa. As area-mean RH is still negative at this level at this time (Fig. 7c), this is likely related to a greater variability within the box. The enhancement in q_c in the low-level cloud deck increases and rises until 09 UTC. After 09 UTC the more dynamic evolution of the daytime PBL in $f_{op} = 0.1$ leads to a more elevated low-level cloud deck containing more q_c in the vertical column. This denotes a negative feedback mechanism, as a (here enforced) reduction of low cloud opacity leads to more cloud production,

at least in the early part of the day. Recall that the modification was only applied to the cloud optical thickness, as seen by the radiation scheme.

Finally, Fig. 7f shows impacts on horizontal winds. As already mentioned above, the $f_{op} = 0.1$ experiment has a stronger NLLJ developing around 18 UTC and lasting through the night. Only 12 and 15 UTC, when mixing is strongly increased (Fig. 7d), show a reduction of low-level wind speed. Above that, at the level of the African easterly jet (750–450 hPa) and at the level of the tropical easterly jet (300–150 hPa), v_{horiz} is markedly decreased, a signal with a relatively small diurnal cycle. One possible explanation for this finding is a reduction of wind peaks through increased convective mixing, depositing more momentum in the layer of lower background winds at 400 hPa.

Figure 8 shows the corresponding profiles for PARAM. Despite the overall consistent signal in rainfall and radiation as documented in Fig. 4, there are many substantial differences between the two sets of experiments.

Despite a larger SSI (see Fig. 4a), PARAM has a lower daytime increase in near-surface temperature, particularly at 15 and 18 UTC, suggesting a possible impact of the earlier triggering of convection in PARAM (see Fig. 5). Near surface q_v (Fig. 8b) is strongly decreased at 09 UTC, probably due to the earlier onset of PBL mixing with transparent clouds, and then strongly increased at 12 and 15 UTC, possibly due to the lack of deep mixing as in EXPL, leading to very large differences between the two sets of experiments. Combined, the changes in temperature and moisture lead to overall less pronounced changes in RH at low levels (both negative near the surface and positive above; Fig. 8c), associated with mostly negative changes in q_c (Fig. 8e) except for 09 UTC. These explain the somewhat unexpected results for q_c discussed in the context of Figs. 7 and 6. In contrast to EXPL, PARAM operates a positive feedback mechanism, where a reduction in low cloud leads to a further reduction. This may clarify, why so many climate models show very large negative biases in cloud cover (Hannak et al., 2017).

Increased vertical mixing can be observed via TKE (Fig. 8d). Positive signals are restricted to the low levels during the day (09, 12 and 15 UTC), with the latter time showing indications for increased mixing reaching midlevels. All hours from 18 UTC to 09 UTC show decreased TKE below 600 hPa and hardly any change at all above that. One needs to bear in mind, however, that the mixing through convection is not reflected in TKE fields in PARAM. Nevertheless, the PARAM signals, at least at low levels, are in clear contrast to EXPL (Fig. 7d) where TKE increases everywhere. These differences are strong indicators that the interplay between PBL turbulence, shallow and deep convection fundamentally differs between the two model configurations. Particularly during nighttime, PARAM shows a slight stabilization in the temperature profile (Fig. 8a) above 925 hPa that appears to suppress turbulence generation in this layer. This cooling may be related to the enhanced NLLJ (Fig. 8f), but it is not clear why this effect does not work in EXPL, where an even more enhanced NLLJ and also a stabilization is observed (Figs. 7a and f). The changes in mixing have profound impacts on many low-level fields, whereas more agreement between EXPL and PARAM is found at mid- and upper-levels, except for some changes in the diurnal cycle.

Overall this discussion demonstrates the enormous importance of vertical transport and mixing in a moist tropical environment where the PBL, low clouds and deep convection are closely coupled through radiative effects.

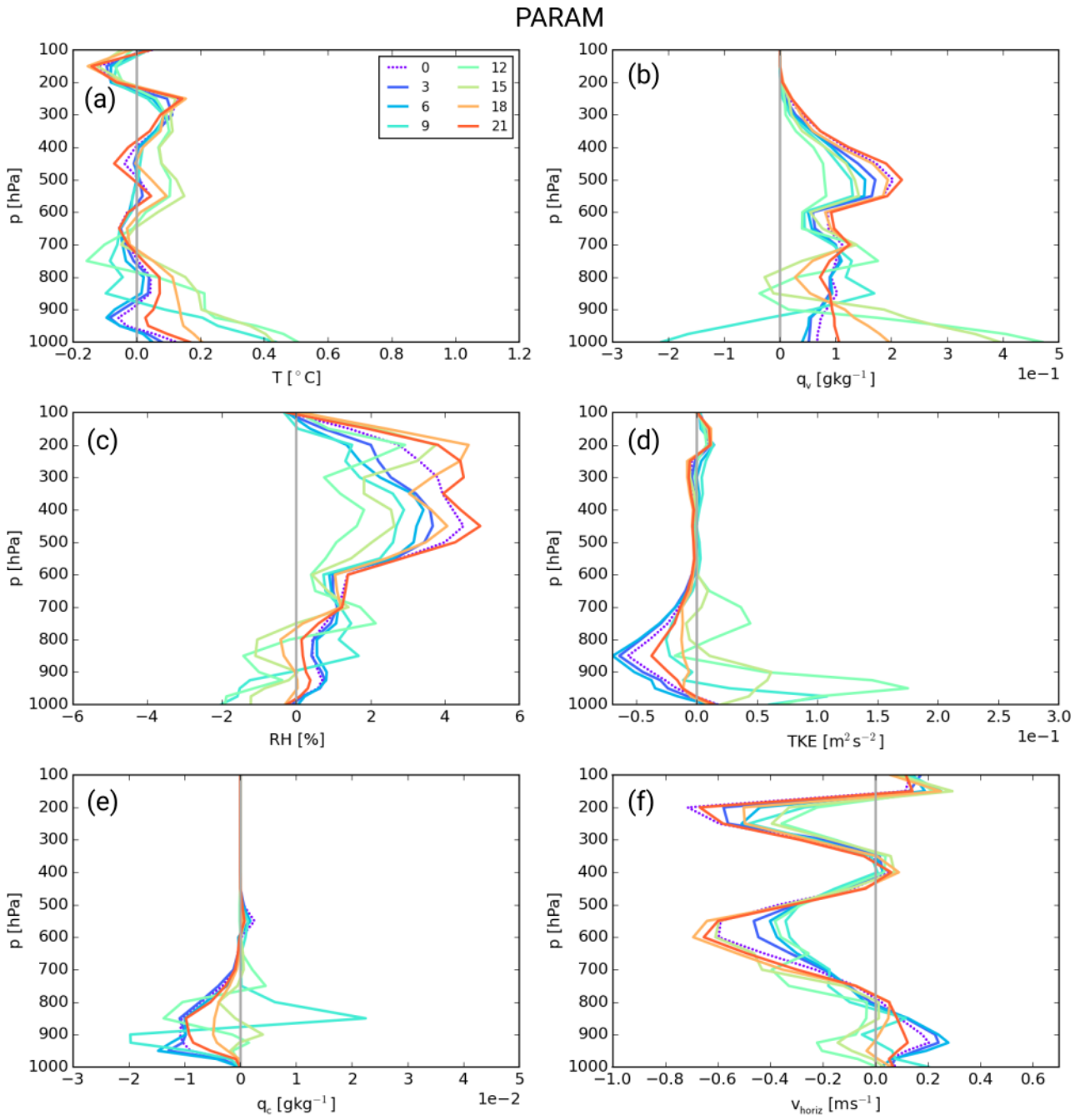

Figure 8. As Fig. 7 but for PARAM.

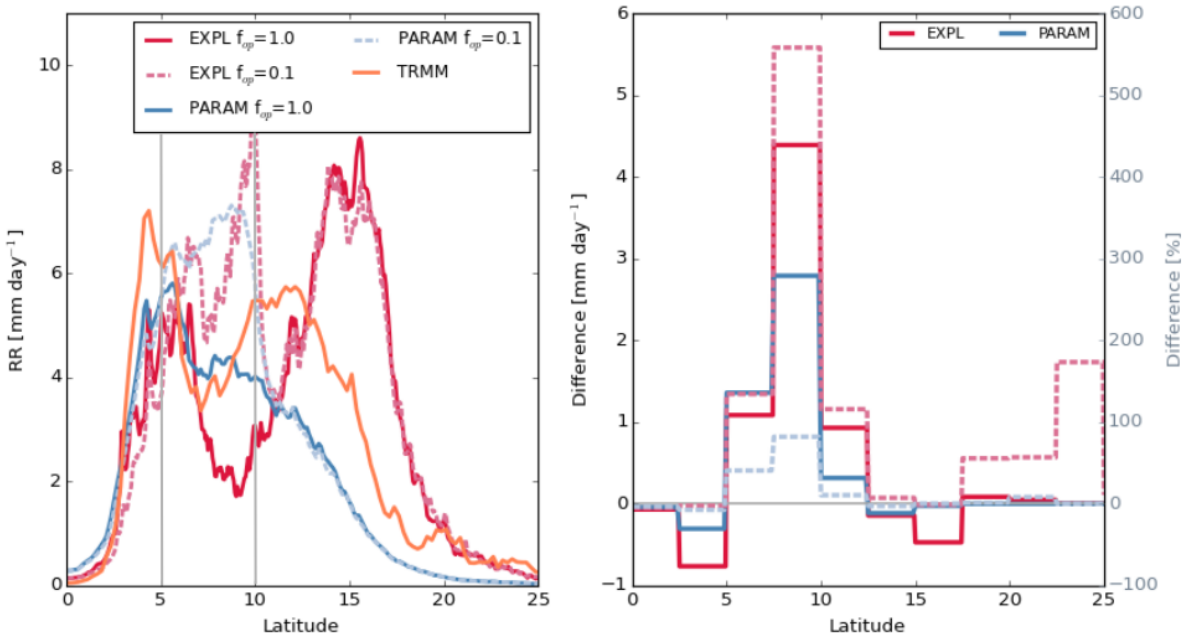

Figure 9. South–north distribution of 8°W–8°E averaged RR from various ICON simulations and TRMM observations (according to the legend) for July 2006: (a) absolute amounts and (b) differences $f_{op} = 0.1$ minus $f_{op} = 1.0$ as absolute (solid) and relative (dashed) values. For better visibility, the data points were binned every 2.5° latitude in (b).

3.4 Regional impact

3.4.1 Precipitation

The previous sections have revealed how moderate reductions in low-level cloud opacity can profoundly change the diurnal cycle in many meteorological variables over southern West Africa, leading amongst other things to a substantial increase in precipitation. This raises the question to what extent these modifications have an impact on neighboring regions or even on the entire WAM system. Does the increased precipitation over the DACCIWA box suppress precipitation to the north and south? Does this enhance or weaken the monsoon circulation? To answer these questions, we expanded the analysis of the sensitivity experiments and included the Sahel zone up to about 25°N.

Figure 9a shows zonally averaged (8°W–8°E) south–north distributions of precipitation for the ICON EXPL and PARAM experiments with $f_{op} = 0.1$ and $f_{op} = 1.0$ together with the corresponding TRMM observation, while Fig. 9b displays the sensitivities in absolute and relative terms. Despite the differences in EXPL and PARAM, the response to reducing the cloud optical thickness is similar, with a large increase over the modification region itself (5–10°N) and immediately to the north, i.e. downstream with the monsoon flow, and rather small changes elsewhere. For PARAM differences outside of the DACCIWA

box are small in both an absolute and relative sense (Fig. 9b). Largest differences occur in the northern half of the box with an increase of almost 3 $\mathrm{mm\ day^{-1}}$ corresponding to about 80%. For $f_{op} = 3.0$ and $f_{op} = 10.0$ (not shown in Fig. 9) decreases in rainfall can be observed outside of the DACCIWA box, but are almost undistinguishable from the control experiment.

Changes in EXPL are generally more dramatic. Given the drier conditions over the Guinea Coastal region in the control run, the increase of almost 4.5 $\mathrm{mm\ day^{-1}}$ in the northern half of the DACCIWA box corresponds to 560%, while the southern half of the box and the 2.5°-strip to the north of it still reach increases on the order of 100%. To the north and south of that, small decreases in absolute values are found, most likely due to an immediate suppression by the enhanced convection in the box, but these are barely significant in a relative sense (Fig. 9b). Finally, to the north of 17.5°N there is a small increase in absolute values, which, given the increasingly dry conditions in this area, corresponds to considerable relative changes.

This may suggest that modulations to the WAM allow a slightly deeper penetration of rainfalls into the continent. However, given that in the northern Sahel rainfall is usually caused by few distinct, intense convective systems and that soil moisture perturbations become increasingly important, five-day simulations during one month is probably insufficient to make any definite statements for this area.

3.4.2 WAM system

In order to better understand these precipitation signals, Fig. 10 shows corresponding south–north distributions of differences between the two EXPL runs for various meteorological quantities and their diurnal variations. Despite the relatively small impacts on precipitation, it demonstrates that the influence of the low cloud manipulation is not restricted to the manipulated area itself (dark grey lines) but is transported northwards with the mean flow as proposed by Zheng et al. (1999). This is evident, for example, for temperature at 975 hPa, T_{975} (Fig. 10a). The near-surface heating peaks at 15 UTC within the box reaching values well above 1.0 $°C$ apart from the southernmost part, where inflow from the ocean creates cooling. Until 06 UTC the T_{975} signal weakens in magnitude and drifts northward out of the DACCIWA box. This change in advection (possibly in addition to radiative changes) leads to an overall moderate warming of the 10–20°N strip with a maximum at the end of the night. Farther to the north, there is a moderate decrease in the afternoon, likely connected to the increase in rainfall in this area (see Fig. 9b). The very small T_{975} decrease over the ocean could come from enhanced sensible heat fluxes over the cool coastal waters caused by stronger winds (see Fig. 10c).

The increase in low-level temperature and higher-level latent and radiative heating (see Fig. 7a) leads to a considerable decrease in surface pressure, p_{sfc}, peaking at 18 UTC with decreases of more than 0.6 hPa (Fig. 10b). This effect is clearly spreading downstream of the box as for T_{975} (Fig. 10a) but also upstream, likely due to upper-tropospheric flow. Given the overall north–south pressure difference of the monsoon, this signal leads to a sharpening of the gradient near the coast and a weakening towards the Sahel. The change in pressure creates a marked signal in low-level circulation, represented here by the meridional wind at 925 hPa, v_{925} (Fig. 10c). Southerly winds into and within the box are enhanced by 1 $\mathrm{ms^{-1}}$ and more, particularly leading to an increased NLLJ, while the export towards the Sahel is reduced. Assuming a similar behaviour also in models with parametrized convection, these processes may explain, why an underestimation of low clouds is often found together with an overestimation of NLLJ for many climate models (Knippertz et al., 2011; Hannak et al., 2017) but

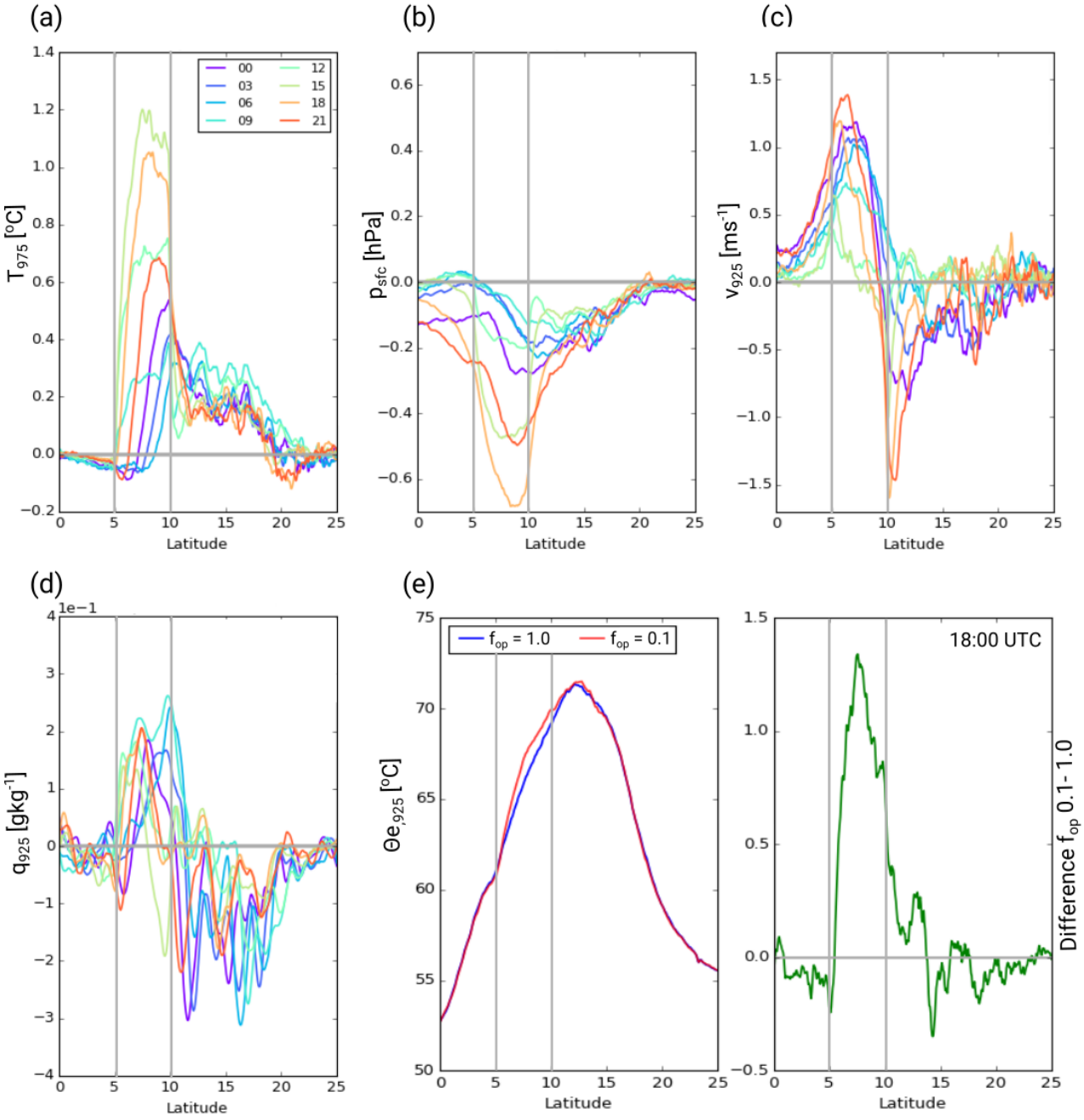

Figure 10. South–north distribution of 8°W–8°E averaged differences of ICON EXPL $f_{op} = 0.1$ minus $f_{op} = 1.0$ for July 2006. Colored lines provide a 3-hourly resolution of the diurnal cycle of (a) T, (b) p_{sfc}, (c) meridional wind v and (d) q_v. In (e) absolute θ_e curves and their difference are shown. Apart from p_{sfc} and T at 975 hPa, all variables are shown for 925 hPa.

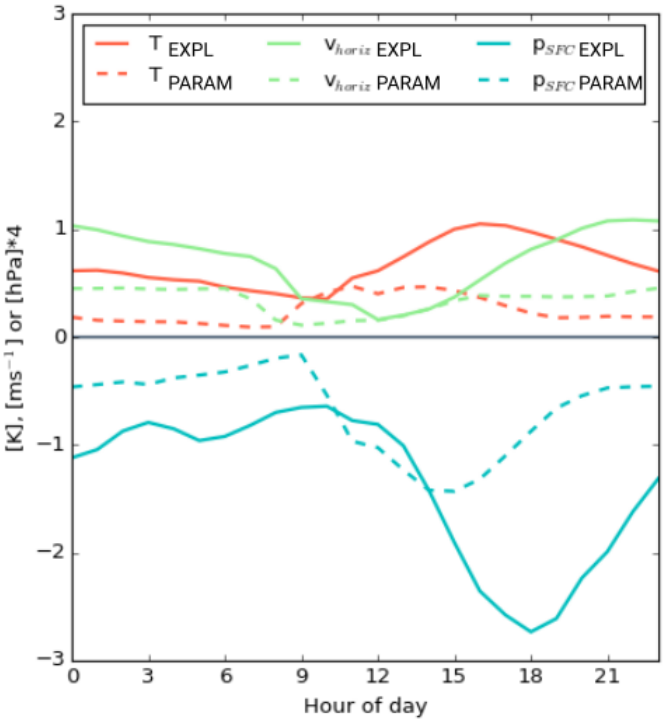

Figure 11. Maximum hourly value extracted from south–north distributions of July 2006 averaged diurnal cycles in Figs. 10 and 13 for T and v_{horiz} at 925 hPa as well as p_{sfc} (according to legend).

this needs further study. Wind signals generally tend to be smaller during the day when PBL turbulence creates a drag on the monsoon circulation (e.g. Parker et al., 2005; Marsham et al., 2013). These changes in circulation also explain the strong moisture convergence into the DACCIWA box discussed above. In addition to the meridional component shown here, there is also strongly enhanced moisture convergence in the zonal flow in response to the reduced pressure (not shown). Enhanced evaporation due to stronger winds over the ocean (Fig. 10c) may also make a contribution. The link between temperature, pressure and wind is further illustrated in Fig. 11 that shows extrema in the south–north profiles of Figs. 10a–c for each hour. T_{975} signals clearly lag the diurnal cycle of solar radiation and peak around 16 UTC. Due to the additional effect of latent heating by convection, the p_{sfc} minimum is reached with a delay of about 2 hours. Finally v_{925} is even further delayed peaking around 22 UTC, when the increase in pressure gradient is still large but when daytime turbulence has died down.

The response in low-level moisture, represented here by q_v at 925 hPa (Fig. 10d) shows a relatively complicated pattern. Signals within the DACCIWA box are predominantly positive, as already discussed, showing some signs of nocturnal advection to the north similar to T_{975} (Fig. 10a). Upstream over the ocean, q_v is almost unchanged but downstream values are reduced almost everywhere at all times of day with largest differences during the night. This is unlikely a purely advective signal and is

suspected to be partly caused by local vertical mixing. To further investigate this point, Fig. 12 shows vertical profiles of the q_v signal at 00 and 12 UTC with the DACCIWA box and the 925-hPa level indicated by grey lines. At midnight (Fig. 12a), when daytime convection dies down, a deep atmospheric moistening with values of up to 0.6 gkg^{-1} is found in the DACCIWA box and immediately to the north of it. The near-surface layer shows both positive and negative contributions. Upstream over the ocean moderate drying occurs in the 800 to 900 hPa layer, possibly related to enhanced subsidence in this area in response to the convective enhancement over land (this signal is clearly stronger at 00 UTC than at 12 UTC). The area to the north of the DACCIWA box shows little signal above 700 hPa but an overall drying below with two local minima around 12 and 15°N. Where do these minima come from? A possible clue is provided by the signals at 12 UTC shown in Fig. 12b. The deeper mixing in the DACCIWA box with optically thinner low clouds creates an earlier PBL build-up, mixing moisture from lower to midlevels, as already discussed (see Fig. 7b). While southern areas in the DACCIWA box receive "fresh" moisture from the ocean, the low-level dry air is advected northward with the monsoon flow and reaches 12°N by 00 UTC (Fig. 12a) subject to some vertical mixing. In the same way, the dry signal at 15°N at 00 UTC would originate in the DACCIWA box 36 hours earlier and the dry signal at 17.5°N at 12 UTC 48 hours earlier. An additional factor could be that the warmer low levels in this area (Fig. 10a) enhance vertical mixing and therefore entrainment of drier air into the PBL advected westward with the African easterly jet. Above this drier surface layer, the 12-UTC profile shows a moistening between 10 and 13°N that supports the idea of deeper mixing but possibly also some advection in the deep southerly monsoon flow. Through compensation, column moisture does not change much in this zone and rainfall even increases (Fig. 9). From this discussion the observed small precipitation increase to the north of 17.5°N (Fig. 9) is not clear but a more detailed investigation is beyond the scope of this paper.

Finally, we would like to address the question of how the low clouds over southern West Africa affect the overall monsoon circulation. As mentioned in the Introduction, a well established conceptual model for this is the theoretical framework proposed by Eltahir and Gong (1996), Zheng et al. (1999) and others, which relates the strength of the circulation to the large-scale meridional gradient in equivalent potential temperature θ_e within the PBL, assuming sufficient deep mixing by convection (e.g. Emmanuel, 1995; Nie et al., 2010). In order to apply this idea to our sensitivity experiments, Fig. 10e shows south–north distributions of θ_e at 925 hPa as absolute values (left) and as differences (right). As described by many studies, the monsoon is related to a large θ_e difference of almost 20 $^\circ C$ between the equator and about 12.5°N. Despite the large local impacts discussed so far, our low-cloud modifications do not perturb this large-scale gradient significantly. Upstream changes are practically negligible. In the area of the θ_e maximum, changes remain well below 0.5 $^\circ C$, resulting from the increase in temperature but decrease in low-level moisture. This is considerably smaller than observed interannual variations of 1–2 $^\circ C$ (e.g. Hurley and Boos, 2013) and consistent with the relatively small impact on precipitation in the Sahel evident from Fig. 9. In the DACCIWA box itself and immediately downstream, however, the combined increase of temperature and moisture leads to θ_e changes of more than 1 $^\circ C$ and a strong local precipitation increase. This means that the reduction of the effective albedo over southern West Africa allows concentrating more energy and precipitation over land without the necessity of shifts between land areas. An interesting implication of this result is that whatever change in aerosol-radiation or aerosol-cloud interaction is

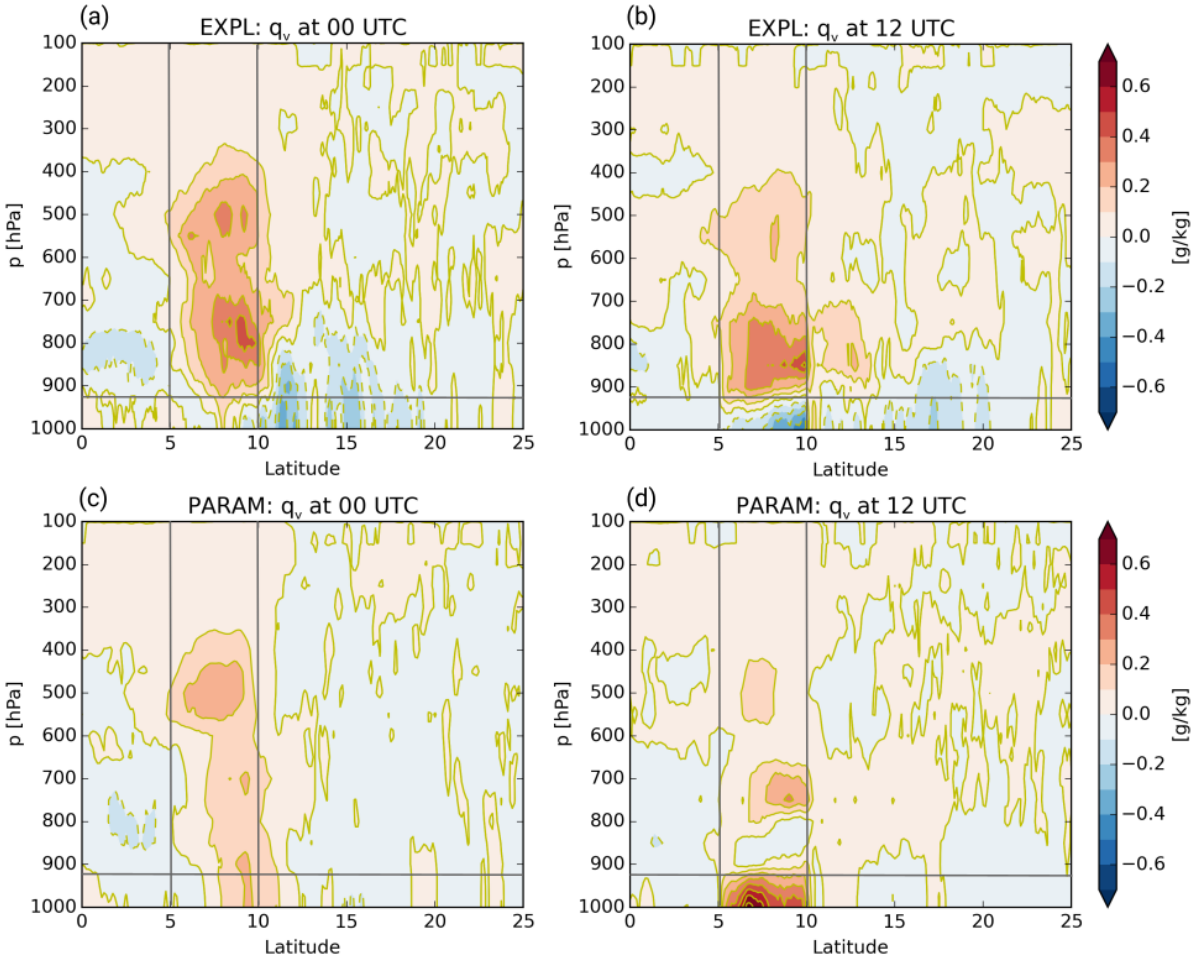

Figure 12. South–north distribution of 8°W–8°E averaged q_v differences of ICON EXPL (top) and PARAM (bottom) $f_{op} = 0.1$ minus $f_{op} = 1.0$ for July 2006. Left panels show for 00 UTC and right panels 12 UTC. Grey lines indicate the borders of the DACCIWA box and the 925 hPa level used in Figs. 10 and 13.

caused through changes in anthropogenic emissions in the DACCIWA region, it will likely have measurable local impacts but probably no significant ramifications elsewhere.

This quite noticeable impact was found in the simulations with explicitly simulated convection. The influence of parametrization of convection in this experiment will be discussed next. For comparison, Fig. 13 shows the same fields as displayed in Fig. 10 but for PARAM. It clearly demonstrates the substantially smaller impact of reducing the optical thickness of low clouds on low-level fields within and beyond the DACCIWA box and the substantial changes to the diurnal cycle of the differences. The temperature signal (Fig. 13a) has a much smaller amplitude than in EXPL and peaks earlier in the day as discussed in the context of Fig. 8. Due to the main advection during the night, the impact on the Sahel is even further reduced and shows even

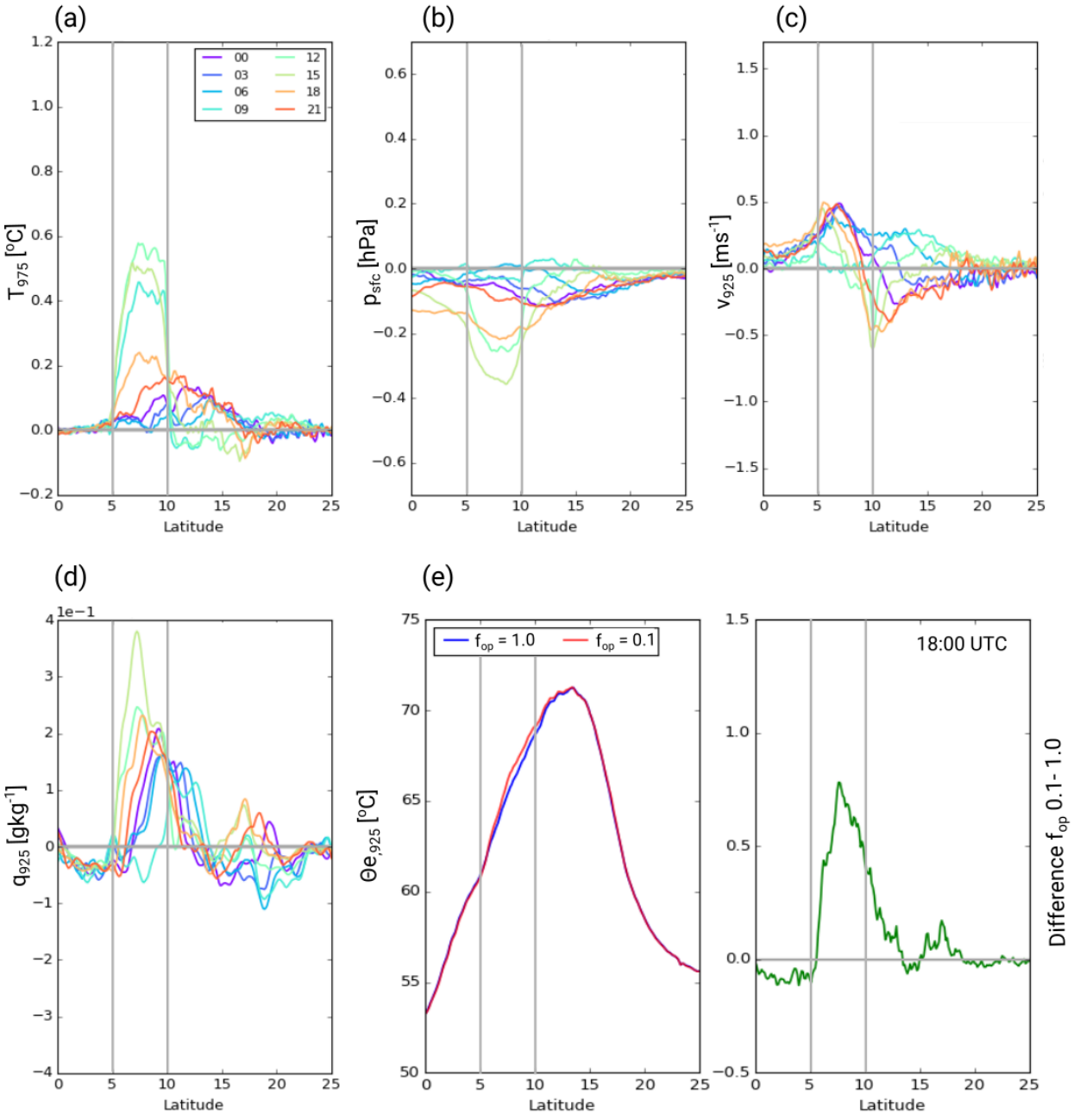

Figure 13. As Fig. 10 but for PARAM.

a slight cooling during daytime. A similar behavior is found for p_{sfc} (Fig. 13b) with a smaller and earlier peak and less impact on the Sahel than in EXPL. Given the relation of pressure and wind, it is no surprise to find a much reduced (or even reversed)

signal in v_{925} also (Fig. 13c). These differences are further illustrated in Fig. 11, showing the much flatter diurnal cycle in temperature with an earlier, less pronounced peak already before midday (red curves). The pressure signal (blue curves) has a larger amplitude, as it is also related to latent heating at upper levels but due to the different timings in precipitation (Fig. 5), a shift of 3 hours relative to EXPL is found. With the pressure signal already much decreased around sunset, the wind response is weak (see also the discussion in Marsham et al., 2013) and shows very little diurnal variations (green curves).

With respect to q_v at 925 hPa, differences between PARAM and EXPL are again more complicated. There is more consistent drying over the ocean in PARAM but moistening with a similar magnitude compared to EXPL in the DACCIWA box (Fig. 13d), however, with a much different diurnal cycle as discussed in the context of Fig. 8. Over the Sahel, the increase in meridional wind (Fig. 13c) during the night leads to a clearer signal of northward moisture advection in stark contrast to EXPL where substantial drying is found (Fig. 10d). Looking at the vertical structure of these signals (Fig. 12) underlines the paramount importance of vertical transports and mixing of moisture. PARAM has generally weak signals everywhere to the north of the DACCIWA box apart from the stronger low-level moisture advection at night and does not show signs of the diurnal pulses of dry advection discussed for EXPL above (Fig. 12c). Over the ocean to the south there is some agreement between PARAM and EXPL on a general drying of low- and midlevels. In the box itself, contrasts are extremely large at 12 UTC. At this time, EXPL shows effects of enhanced nighttime dry advection from the ocean at low levels and moisture left over from convective mixing from the previous day above 925 hPa (Fig. 12b). In PARAM convection is already active at this time, effectively removing tropospheric surplus moisture and depositing it in the PBL (Fig. 12d). Due to the less effective vertical transports during the day in PARAM, the moisture signal at midnight is substantially weaker in the free troposphere (cf. also Figs. 7b and 8b). These changes lead to an overall smaller signal in θ_e at 925 hPa within the DACCIWA box and to the north of it, too (Fig. 13e), apart from the $10-12^{\circ}$N band, where nocturnal moisture advection is enhanced, as discussed above.

Finally, we also tested the time needed for the atmosphere to return to a normal state after a switch-off of the induced cloud changes in the model using the EXPL configuration. These experiments show that low-level variables such as surface radiation and temperature react almost immediately to changes in low cloud during the day. Low-level cloud cover and rainfall respond after one full diurnal cycle, while impacts on higher levels and more remote regions can last days. Impacts on higher levels and more remote regions can last for days but the signals hardly stand out from the high level of background variations indicating the chaotic nature of the atmosphere. More details can be found in the Supplementary Material.

In conclusion, this discussion shows that the parametrized treatment of convection not only affects the diurnal timing of precipitation but also impacts strongly on vertical mixing. Through a number of different mechanisms, these create substantial differences in thermodynamic environments and ultimately in the sensitivity to modifications of low-level clouds, which is generally higher in EXPL than PARAM. The differences also impact on the propagation of signals to the Sahel in both magnitude and diurnal timings. Despite all this, precipitation signals are clearly dominated by the DACCIWA box itself with only minor impacts outside of the box.

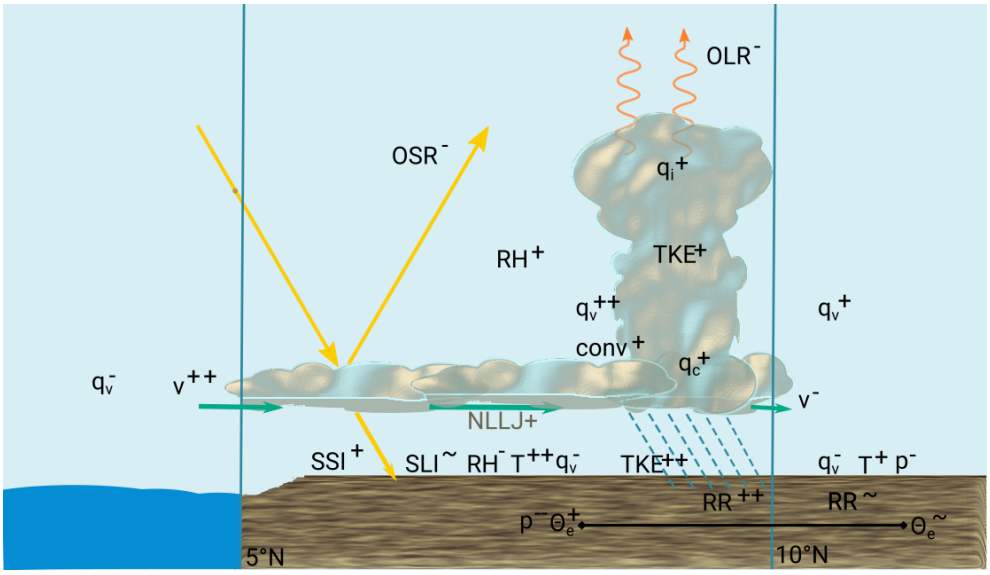

Figure 14. Conceptual sketch of the most important changes when reducing the optical thickness of low clouds based on the ICON EXPL experiments. For more details see Sect.
4.

4 Conclusions

In the present study, we analyzed the role of low-level clouds over southern West Africa on the local meteorology and larger monsoon system. They frequently form during the night close to the surface and often persist long into the following day. At their maximum diurnal extent, they cover a vast area of about 850 000 km^2 in southern West Africa (van der Linden et al., 2015). Their formation is linked to cold advection and turbulent mixing associated with the NLLJ and radiative cooling (Schrage and Fink, 2012; Schuster et al., 2013; Kalthoff et al., 2018). These clouds play an important role in the energy budget and diurnal cycle during summertime and tend to be badly represented in many climate models (Hannak et al., 2017). The role of these clouds in the WAM system was assessed here for the first time in a fully nonlinear way via sensitivity experiments using the ICON model from the DWD in NWP mode for July 2006. Cloud radiative effects were suppressed or enhanced in the model over the main low-level stratus region 5–10°N and 8°W–8° by multiplying q_c below 700 hPa with a constant factor f_{op} before the call of the radiation scheme. Simulations with a horizontal grid-spacing of 13.2 km and parametrized moist convection (PARAM) were systematically compared to those with an additional nest over West Africa with a finer grid-spacing of 6.6 km and explicit convection (EXPL).

Comparisons with ground and satellite-based observations of rainfall and radiation show substantial deviations between the two model configurations and with the observations. PARAM reproduces the coastal rainfall maximum over the Niger Delta but struggles to represent the inland penetration of precipitation. It appears to have realistic SSI but too much extinction of shortwave radiation in the atmosphere, leading to a negative bias in OSR. EXPL also reproduces the coastal rainfall well but

in contrast to PARAM has a much too strong Sahelian rainband substantially further north than observed. EXPL appears to have slightly too many low clouds, leading to reduced SSI and increased OSR. PARAM generally tends to have substantially more high and less low clouds compared to EXPL. This demonstrates the enormous influence of convective parametrisation on the West African meteorology as already documented in Marsham et al. (2013). As both model configurations show marked disagreement with observations, a quantitative interpretation of the results appears questionable. However, we argue that we can still use the model to investigate which sensitivities are robust and how convective parametrization modifies the sensitivity and the involved physical mechanisms.

Making low clouds more transparent to short- and longwave radiation creates a complicated atmospheric response. To summarize the main effects, Fig. 14 shows a schematic overview that reflects the changes found for EXPL, as this experiment shows a more realistic diurnal cycle. Differences to PARAM will then be discussed below. Figure 14 concentrates on daily mean effects but at least for some parameters diurnal variations will be discussed, too. Note that in the NWP simulations SSTs stay largely constant during the short run time; they are initialised with ERA-I, but not updated during a 5-day simulation. The southern and northern borders of the box with cloud modifications, i.e. 5 and 10°N, are marked by vertical lines in Fig. 14.

The first and most obvious aspect is that more transparent low clouds lead to more solar radiation reaching the ground (SSI^{+}) and less being reflected to space (OSR^{-}) during daytime. This leads to an increase in low-level temperature in the daily mean, but particularly during the afternoon (T^{++}). The associated decrease in stability triggers more turbulent mixing (TKE^{++}) and more deep convection ($conv^{+}$), leading to more convective mixing and a substantial increase in precipitation (RR^{++}). Particularly in the northern half of the modification region, rainfall increases by an impressive factor of 5! The almost logarithmic dependence of rainfall on f_{op} illustrates the strong and dominating control the low clouds exert on the triggering of convection. The increase in low-level temperature and free-tropospheric latent heating leads to a marked decrease in surface pressure, particularly around the convective peak at 18 UTC (p^{--}). This in turn sharpens the gradient to the south and creates and enhanced low-level jet over southern West Africa ($NLLJ^{+}$) and a stronger inflow from the Atlantic (v^{++}). At the same time, the export to the Sahel is somewhat reduced (v^{-}). This enhancement in meridional convergence concentrates moisture over southern West Africa and through the enhanced vertical mixing moistens the upper levels (${q_v}^{++}$). As this largely dominates over temperature effects, relative humidity (RH^{+}), cloud water (${q_c}^{+}$) and cloud ice (${q_i}^{+}$) are increased throughout the free troposphere. Only close to the surface and particularly during the day, the enhanced advection of dry subsided air (Schuster et al., 2013) from the ocean and intensified mixing creating a deeper PBL, leads to lower absolute (${q_v}^{-}$) and relative humidity (RH^{-}). At 18 UTC this also leads to less cloud cover and cloud water (not shown). At other times of day, the stronger NLLJ and the additional moisture lead to an increased cover and water content of low clouds, creating a negative feedback. Due to the increase in convection and high clouds, less longwave radiation is emitted to space (OLR^{-}), while surface longwave effects are small due to the overall very moist and cloudy column ($SLI^{\sim}$). The latter is a strong indication of dynamic adjustments in the model. A recent study by Hill et al. (2018) estimated the effect of low clouds over southern West Africa from pure radiative transfer simulations on satellite-derived cloud data. While for the shortwave component (i.e. SSI and OSR) both approaches point in the same direction, the longwave components are reversed.

Effects outside of the cloud modification box are substantially smaller (Fig. 14). Upstream over the ocean the most significant signal is a free tropospheric drying, possibly from enhanced subsidence related to the increase convection over adjacent land. Downstream over the Sahel, low-level advection with the southerly monsoon flow is a dominating effect. Despite the lower meridional wind speeds, the enhanced temperature and lower pressure from the south create impacts as far north as 20°N (T^+ and p^-). With respect to moisture, however, changes in southerly advection, low-level moisture content in the south and deeper mixing caused by the higher near-surface temperatures lead to a drying of low levels (${q_v}^-$), with a diurnal pulsing signature. Above the PBL, however, some of the increased humidity in the south is advected towards the Sahel with the deep monsoon flow (${q_v}^+$), leading to overall small changes in column moisture. Consistent with that and despite the many changes discussed, total rainfall over the Sahel is not strongly affected by the cloud modifications applied here ($RR^\sim$), apart from the immediate vicinity of the box. However, it is possible that the observed changes could still lead to differences in diurnal cycle and/or organization of convection. Hints to the organisation of convection can be found indeed in our model results, the variance of q_v profiles is bigger for EXPL than for PARAM. However, the number of mesoscale convective systems per month is too small to draw any substantial conclusions from the modelled time period. The opposite signs of temperature and moisture changes over the Sahel lead to relatively small changes in low-level θ_e there (${\theta_e}^\sim$), in contrast to southern West Africa, where θ_e is enhanced (${\theta_e}^+$). An interesting implication of this is that the total magnitude of the north–south gradient in this quantity is not affected, which has been shown to be an important control of the overall monsoon circulation (Eltahir and Gong, 1996; Zheng et al., 1999; Hurley and Boos, 2013). Therefore these results strongly suggest that errors or changes to low-level clouds over southern West Africa will likely have substantial local impacts but probably do not strongly affect neighboring regions, at least not in terms of rainfall.

A systematic comparison of the effects described for EXPL with the help of Fig. 14 reveals substantial differences when convective parametrization is used (PARAM). While the first-order effect on rainfall (strong increase over cloud modification box and little impact elsewhere) is confirmed, differences in thermodynamic variables and the diurnal cycle are substantial. First of all, PARAM's diurnal cycle in rainfall is shifted forward by about 3 hours as in many models with parameterized convection (Marsham et al., 2013). This impacts on the sensitivity to low clouds in manifold ways. The low-level heating with more transparent clouds is reduced leading to reduced pressure and wind signals. Reduced and differently timed vertical mixing has large impacts on the diurnal cycle of the vertical distribution of moisture. This is most extreme at midday when PARAM has a marked low-level increase of moisture with transparent low clouds, related to more convective rainfall, while EXPL has a marked decrease from stronger dry advection and PBL mixing. These differences lead to an overall decrease of low clouds and cloud water in PARAM in contrast to an increase in EXPL for most times of day. This unexpected positive feedback can serve as an explanation, why many models with convective parametrization show large negative biases in low-level cloud cover (Knippertz et al., 2011; Hannak et al., 2017). In addition, exports of temperature and moisture signals to the Sahel are reduced and follow a different timing.

In conclusion, this study has for the first time demonstrated the enormous control of the persistent and widespread low clouds over southern West Africa on local rainfall, while impacts on neighbouring regions are moderate at best. These results suggest that the well documented low-cloud errors in many climate models (Hannak et al., 2017) can likely serve as an explanation for

the often large precipitation errors in the Guinea Coastal region but not in the Sahel, a least not in terms of average amount. Similar effects can be expected from changes in low-level aerosol, as already documented for a case study by Deetz et al. (2018a). Increases in aerosol optical thickness, e.g. through human activity, would therefore reduce precipitation in the region affected by the stratus. Such increases in anthropogenic activity have been observed and are projected to increase given the overall dynamic population and economic development (see Knippertz et al., 2015). It would be desirable to explicitly model this effect for longer periods using convection permitting resolution. A detailed treatment of aerosol processes, including wet deposition and water uptake (Deetz et al., 2018b) will be required for a realistic representation of the problem. A suppression of rainfall by aerosols could create a positive feedback by reducing wet removal. In addition, more work is needed to gauge the realism of the simulations used for this study. While comparisons with rainfall and radiation are presented here, it would be necessary to also evaluate low-level thermodynamic and dynamic fields. The recent DACCIWA field campaign (Flamant et al., 2018) has generated an exciting new dataset to make progress on this end, particularly through its extensive ground-based measurements (Kalthoff et al., 2018). In the long run, it is hoped that these activities can improve weather and climate models over this crucial and densely populated region, as there is no hope to realistically model the local meteorology without a realistic representation of the diurnal behaviour of low clouds.

Competing interests. The authors declare no competing interests.

Acknowledgements. The authors acknowledge insightful input from Raphaela Vogel and one anonymous reviewer that helped improve an earlier version of the manuscript.

The research presented in this article has received funding from the European Union 7th Framework Programme (FP7/2007-2013) under Grant Agreement 603502 (EU project DACCIWA: Dynamics–Aerosol–Chemistry–Cloud Interactions in West Africa). Radiation measurements at Cotonou and Parakou were carried out by the IMPETUS project funded by the BMBF project IMPETUS (BMBF Grant 01LW06001A, North Rhine-Westphalia Grant 313-21200200). We particularly thank Orou Goura Doussi and Michael Christoph for their maintenance and data retrieval commitment for the Parakou station. We wish to thank Abdourahamane Konaré, Adama Diawara, and Fidèle Yoroba for providing the radiation data from the Lamto Geophysical Observatory in Ivory Coast. The dataset SARAH from EUMETSAT's Satellite Application Facility on Climate Monitoring was used to evaluate the ICON model, as well as CERES and TRMM data from NASA.

References

Adler, B., Kalthoff, N., and Gantner, L.: Nocturnal low-level clouds over southern West Africa analysed using high-resolution simulations, Atmos. Chem. Phys., 17, 899-910, https://doi.org/10.5194/acp-17-899-2017, 2017.

Adler, R. F., Huffman, G.J., Chang, A., Ferraro, R., Xie, P., Janowiak, J., Rudolf, B., Schneider, U., Curtis, S., Bolvin, D., Gruber, A., Susskind, J., Arkin, P., and Nelkin, E.: The Version-2 Global Precipitation Climatology Project (GPCP) monthly precipitation analysis (1979–present), J. Hydrometeor., 4, 1147–1167, https://doi.org/10.1175/1525-7541(2003)004<1147:TVGPCP>2.0.CO;2, 2003.

Barker, H.W., Marshak, A., Szyrmer, W., Blanchet, J., Trishchenko, A., and Li, Z.: Inference of cloud optical depth from aircraft-based solar radiometric measurements, J. Atmos. Sci., 59, 2093–2111, https://doi.org/10.1175/1520-0469(2002)059<2093:IOCODF>2.0.CO;2, 2002.

Bechtold, P., Köhler, M., Jung, T., Doblas-Reyes, F., Leutbecher, M., Rodwell, M., Vitart, F., and Balsamo, G.: Advances in simulating atmospheric variability with the ECMWF model: From synoptic to decadal time-scales, Q. J. Roy. Meteor. Soc., 134, 1337–1351, 2008.

Boone, A., de Rosnay, P., Balsamo, G., Beljaars, A., Chopin, F., Decharme, B., Delire, C., Ducharne, A., Gascoin, S., Grippa, M., Guichard, F., Gusev, Y., Harris, P., Jarlan, L., Kergoat, L., Mougin, E., Nasonova, O., Norgaard, A., Orgeval, T., Ottlé, C., Poccard-Leclercq, I., Polcher, J., Sandholt, I., Saux-Picart, S., Taylor, C., and Xue, Y.: The AMMA Land Surface Model Intercomparison Project (ALMIP), B. Am. Meteorol. Soc., 90, 1865–1880, https://doi.org/10.1175/2009BAMS2786.1, 2009.

Caniaux, G., H. Giordani, J.L. Redelsperger, F. Guichard, E. Key, and M. Wade: Coupling between the Atlantic cold tongue and the West African monsoon in boreal spring and summer, J. Geophys. Res., 116, C04003, doi:10.1029/2010JC006570, 2011.

Clerbaux, N., Urbain, M., Ipe, A., Baudrez, E., Velazquez-Blazquez, A., Akkermans, T., Hollmann, R., Fuchs, P., Selbach, N., and Werscheck, M.: CM SAF TOA Radiation GERB/SEVIRI Data Record - Edition 2, Satellite Application Facility on Climate Monitoring, DOI:10.5676/EUM_SAF_CM/TOA_GERB/V002, https://doi.org/10.5676/EUM_SAF_CM/TOA_GERB/V002, 2017.

Couvreux, F. , Guichard, F., Gounou, A., Bouniol, D., Peyrillé, P., and Köhler, M.: Modelling of the thermodynamical diurnal cycle in the lower atmosphere: A joint evaluation of four contrasted regimes in the tropics over land, Bound.-Lay. Meteorol., 150, 185–214, DOI 10.1007/s10546-013-9862-6, 2014.

Dee, D. P., Uppala, S. M., Simmons, A. J., Berrisford, P., Poli, P., Kobayashi, S., Andrae, U., Balmaseda, M. A., Balsamo, G., Bauer, P., Bechtold, P., Beljaars, A. C. M., van de Berg, L., Bidlot, J., Bormann, N., Delsol, C., Dragani, R., Fuentes, M., Geer, A. J., Haimberger, L., Healy, S. B., Hersbach, H., Hólm, E. V., Isaksen, L., Kållberg, P., Köhler, M., Matricardi, M., McNally, A. P., Monge-Sanz, B. M., Morcrette, J.-J., Park, B.-K., Peubey, C., de Rosnay, P., Tavolato, C., Thépaut, J.-N. and Vitart, F.: The ERA-Interim reanalysis: configuration and performance of the data assimilation system, Q. J. Roy. Meteor. Soc., 137, 553-597, doi:10.1002/qj.828, 2011.

Deetz, K., Vogel, H., Knippertz, P., Adler, B., Taylor, J., Coe, H., Bower, K., Haslett, S., Flynn, M., Dorsey, J., Crawford, I., Kottmeier, C., and Vogel, B.: Numerical simulations of aerosol radiative effects and their impact on clouds and atmospheric dynamics over southern West Africa, Atmos. Chem. Phys., 18, 9767–9788, doi:10.5194/acp-18-9767-2018, 2018.

Diedhiou, A., Janicot, S., Viltard, A., de Felice, and Laurent, H. P.: Easterly wave regimes and associated convection over West Africa and tropical Atlantic: results from the NCEP/NCAR and ECMWF reanalyses, Clim. Dyn., 15, 11, 795-822, https://doi.org/10.1007/s003820050316, 1999.

Doms, G. and Schättler, U.: A description of the nonhydrostatic regional model LM. Part II: Physical parameterization, Technical report, Deutscher Wetterdienst, Offenbach, http://www.cosmo-model.org/public/documentation.htm, 2004.

Edwards, J. M. and Slingo, A.: Studies with a flexible new radiation code. 1: Choosing a configuration for a large-scale model, Q. J. Roy. Meteor. Soc., 122, 690–719, 1996.

Eltahir, E. A. B., and Gong, C. L.: Dynamics of wet and dry years in West Africa, J. Climate, 9, 1030–1042, 1996.

Emmanuel, K. A.: On thermally direct circulations in moist atmospheres, J. Atmos. Sci., 52, 1529–1534, 1995.

Fein, J. S., Stephens, P. L., and Loughran, K. S.: The Global Atmospheric Research Program: 1979–1982, Rev. Geophys., 21, 5, 1076–1096, doi:10.1029/RG021i005p01076, 1983.

Fink, A. H., Engel, T., Ermert, V., van der Linden, R., Schneidewind, M., Redl, R., Afiesimama, E., Thiaw, W. M., Yorke, C. and Evans, M.: Mean climate and seasonal cycle, in Meteorology of tropical West Africa: The forecasters' handbook, Parker, D. J., Diop-Kane M. (eds.): 1 – 39. Wiley: Chichester, UK. https://doi.org/10.1002/9781118391297.ch1, 2017.

Fitzpatrick, R. G. J., Bain, C., Knippertz, P., Marsham J. H., and Parker, D. J.: The West African monsoon onset – A concise comparison of definitions, J. Climate, 28, 8673–8694, doi:10.1175/JCLI-D-15-0265.1, 2015.

Flamant, C., Knippertz, P., Fink, A. H., Akpo, A., Brooks, B., Chiu, C., Coe, H., Danuor, S.,. Evans, M., Jegede, O., Kalthoff, N., Konaré, A., Liousse, C., Lohou, F., Mari, C., Schlager, H., Schwarzenboeck, A., Adler, B., Amekudzi, L., Aryee, J., Ayoola, M., Batenburg, A. M., Bessardon, G., Borrmann, S., Brito, J., Bower, K., Burnet, F., Catoire, V., Colomb, A., Denjean, C., Fosu-Amankwah, K., Hill, P. G:, Lee, J., Lothon, M., Manaran, M., Marsham, J. H., Meynadier, R., Ngamini, J.-B., Rosenberg, P., Sauer, D., Smith, V., Stratmann, G., Taylor, J. W., Voigt, C., and Yoboué, V.: The Dynamics-Aerosol-Chemistry-Cloud Interactions in West Africa field campaign: Overview and research highlights, B. Am. Meteorol. Soc., 99, 1, 83–104, doi:10.1175/BAMS-D-16-0256.1, 2018.

Haiden, T., Rodwell, M. J., Richardson, D. S., Okagaki, A., Robinson, T., and Hewson, T.: Intercomparison of global model precipitation forecast skill in 2010/11 using the SEEPS score, Mon. Weather Rev., 140, 8, 2720–2733, 2012.

Hall and Perrillé: Dynamics of the West African monsoon, J. Phys. IV, 139, 81-99, doi:10.1051/jp4:2006139007, 2006.

Ham, S.-H., Kato, S., Rose, F. G., Winker, D., L'Ecuyer, T., Mace, G. G., Painemal, D., Sun-Mack, S., Chen, Y., and Miller, W. F.: Cloud occurrences and cloud radiative effects (CREs) from CERES-CALIPSO-CloudSat-MODIS (CCCM) and CloudSat radar-lidar (RL) products, J. Geophys. Res. Atmos., 122, 8852–8884, doi:10.1002/2017JD026725, 2017.

Hannak, L., Knippertz, P., Fink, A.H., Kniffka, A., and Pante, G.: Why do global climate models struggle to represent low-level clouds in the West African summer monsoon?, J. Climate, 30, 1665–1687, https://doi.org/10.1175/JCLI-D-16-0451.1, 2017.

Harries, J.E., Russell, J.E., Hanafin, J.A., Brindley, H., Futyan, J., Rufus, J., Kellock, S., Matthews, G., Wrigley, R., Last, A., Mueller, J., Mossavati, R., Ashmall, J., Sawyer, E., Parker, D., Caldwell, M., Allan, P.M., Smith, A., Bates, M.J., Coan, B., Stewart, B.C., Lepine, D.R., Cornwall, L.A., Corney, D.R., Ricketts, M.J., Drummond, D., Smart, D., Cutler, R., Dewitte, S., Clerbaux, N., Gonzalez, L., Ipe, A., Bertrand, C., Joukoff, A., Crommelynck, D., Nelms, N., Llewellyn-Jones, D.T., Butcher, G., Smith, G.L., Szewczyk, Z.P., Mlynczak, P.E., Slingo, A., Allan, R.P., and Ringer, M.A.: The geostationary earth radiation budget project, B. Am. Meteorol. Soc., 86, 945–960, https://doi.org/10.1175/BAMS-86-7-945, 2005.

Heise, E., Ritter, B., and Schrodin, E.: Operational implementation of the multilayer soil model TERRA, Technical report. Deutscher Wetterdienst: Offenbach, Germany. http://www.cosmo-model.org, 2006.

Hill, P., Allan, R., Bodas-Salcedo. A., and Chiu, C.: Quantifying the contribution of different cloud types to the radiation budget in southern West Africa during the monsoon season, J. Climate, 31, 5273–5291, https://doi.org/10.1175/JCLI-D-17-0586.1, 2018.

Huffman, G.J., Bolvin, D.T., Nelkin, E.J., Wolff, D.B., Adler, R.F., Gu, G., Hong, Y., Bowman, K.P., and Stocker, E. F.: The TRMM Multi-satellite Precipitation Analysis (TMPA): Quasi-global, multiyear, combined-sensor precipitation estimates at fine scales, J. Hydrometeor., 8, 38-55, https://doi.org/10.1175/JHM560.1, 2007.

Hurley, J. V. and Boos, W. R.: Interannual variability of monsoon precipitation and local subcloud equivalent potential temperature, J. Climate, 26, 9507–9527, https://doi.org/10.1175/JCLI-D-12-00229.1, 2013.

Janicot, S., Thorncroft, C. D., Ali, A., Asencio, N., Berry, G., Bock, O., Bourles, B., Caniaux, G., Chauvin, F., Deme, A., Kergoat, L., Lafore, J.-P., Lavaysse, C., Lebel, T., Marticorena, B., Mounier, F., Nedelec, P., Redelsperger, J.-L., Ravegnani, F., Reeves, C. E., Roca, R., de Rosnay, P., Schlager, H., Sultan, B., Tomasini, M., Ulanovsky, A., and ACMAD forecasters team: Large-scale overview of the summer monsoon over West Africa during the AMMA field experiment in 2006, Ann. Geophys., 26, 2569-2595, https://doi.org/10.5194/angeo-26-2569-2008, 2008.

Johnson, R.H., Rickenbach, T.M., Rutledge, S.A., Ciesielski, P.E., and Schubert, W.H.: Trimodal characteristics of tropical convection, J. Climate, 12, 2397–2418, https://doi.org/10.1175/1520-0442(1999)012<2397:TCOTC>2.0.CO;2, 1999.

Kalthoff, N., Lohou, F., Brooks, B., Jegede, G., Adler, B., BabiĆ, K., Dione, C., Ajao, A., Amekudzi, L. K., Aryee, J. N. A., Ayoola, M., Bessardon, G., Danuor, S. K., Handwerker, J., Kohler, M., Lothon, M., Pedruzo-Bagazgoitia, X., Smith, V., Sunmonu, L., Wieser, A., Fink, A. H., and Knippertz, P.: An overview of the diurnal cycle of the atmospheric boundary layer during the West African monsoon season: results from the 2016 observational campaign, Atmos. Chem. Phys., 18, 2913-2928, https://doi.org/10.5194/acp-18-2913-2018, 2018.

Knippertz, P., Fink, A. H., Schuster, R., Trentmann, J., Schrage, J. M., and Yorke, C.: Ultra-low clouds over the southern West African monsoon region, Geophys. Res. Lett., 38, L21808, doi:10.1029/2011GL049278, 2011.

Knippertz, P., Coe, H., Chiu, J. C., Evans, M. J., Fink, A. H., Kalthoff, N., Liousse, C., Mari, C., Allan, R. P., Brooks, B., Danour, S., Flamant, C., Jegede, O. O., Lohou, F., and Marsham, J. H.: The DACCIWA project: Dynamics-aerosol-chemistry-cloud interactions in West Africa, B. Am. Meteorol. Soc., doi: http://dx.doi.org/10.1175/BAMS-D-14-00108.1, 2015.

Knippertz, P., Fink, A. H., Deroubaix, A., Morris, E., Tocquer, F., Evans, M., Flamant, C., Gaetani, M., Lavaysse, C., Mari, C., Marsham, J. H., Meynadier, R., Affo-Dogo, A., Bahaga, T., Brosse, F., Deetz, K., Guebsi, R., Latifou, I., Maranan, M., Rosenberg, P. D., and Schlueter, A.: A meteorological and chemical overview of the DACCIWA field campaign in West Africa in June–July 2016, Atmos. Chem. Phys., 17, 10893–10918. doi:10.5194/acp-17-10893-2017, 2017.

Lafore J.-P., Chapelon, N., Diop-Kane, M., Gueye, B., Largeron, Y., Lepape, S., Ndiaye, O., Parker, D. J., Poan, E., Roca, R., Roehrig, R., and Taylor, C.: Deep convection, in Meteorology of tropical West Africa: The forecasters' handbook, Parker, D. J., Diop-Kane M. (eds.): 90 – 129. Wiley: Chichester, UK. https://doi.org/10.1002/9781118391297.ch3, 2017.

Lavender, S. L., Taylor, C. M., and Matthews, A. J.: Coupled land–atmosphere intraseasonal variability of the West African monsoon in a GCM, J. Climate, 23, 5557–5571, doi: http://dx.doi.org/10.1175/2010JCLI3419.1, 2010.

Leuenberger, D., Koller, M., Fuhrer, O., and Schär, C.: A generalization of the SLEVE vertical coordinate, Mon. Weather Rev., 138, 3683–3689, https://doi.org/10.1175/2010MWR3307.1, 2010.

Li, R., Jin, J., Wang, J., and Gillies, R. R.: Significant impacts of radiation physics in the Weather Research and Forecasting model on the precipitation and dynamics of the West African monsoon, Clim. Dyn., 44, 1583–1594, doi:10.1007/s00382-014-2294-2, 2015.

Loeb, N. G., Wielicki, B. A., Doelling, D. R., Smith, G. L., Keyes, D. F., Kato, S., Manalo-Smith, N., and Wong, T.: Toward optimal closure of the Earth's top-of-atmosphere radiation budget, J. Climate, 22, 748-756, doi: 10.1175/2008JCLI2637.1, 2009.

Lott, F. and Miller, M.: A new subgrid-scale orographic drag parametrization: Its formulation and testing, Q. J. Roy. Meteor. Soc., 123, 101–127, 1997.

Maranan, M. , Fink, A. H., and Knippertz, P.: Rainfall types over southern West Africa: Objective identification, climatology and synoptic environment, Q. J. Roy. Meteor. Soc. Accepted Author Manuscript, doi:10.1002/qj.3345, 2018.

Marsham, J. H., Dixon, N. S., Garcia-Carreras, L., Lister, G. M. S., Parker, G. M. S., Knippertz, P., and Birch, C. E.: The role of moist convection in the West African monsoon system – in- sights from continental-scale convection-permitting simulations, Geophys. Res. Lett., 40, 9, 1843–1849, 2013.

Meynadier, R., Bock, O., Gervois, S., Guichard, F., Redelsperger, J.-L., Agustí-Panareda, A., and Beljaars, A.: West African monsoon water cycle: 2. Assessment of numerical weather prediction water budgets, J. Geophys. Res., 115, D19107, doi:10.1029/2010JD013919, 2010.

Mlawer, E. J., Taubman, S. J., Brown, P. D., Iacono, M. J., and Clough, S. A.: Radiative transfer for inhomogeneous atmospheres: RRTM, a validated correlated-k model for the longwave, J. Geophys. Res., 102, 16, 663–682, doi: 10.1029/97JD00237, 1997.

Mohino, E., Rodríguez-Fonseca, B., Losada, T., Gervois, S., Janicot, S., Bader, J., Ruti, P., and Chauvin, F.: Changes in the interannual SST-forced signals on West African rainfall. AGCM intercomparison, Clim. Dyn., 37, 9/10, 1707–1725, https://doi.org/10.1007/s00382-011-1093-2, 2011.

Mueller, R., Matsoukas, C., Gratzki, A., Behr, H., and Hollmann, R.: The CM-SAF operational scheme for the satellite based retrieval of solar surface irradiance—A LUT based eigenvector hybrid approach, Remote Sens. Environ., 113, 1012–1024, doi:10.1016/j.rse.2009.01.012, 2009.

Müller, R., Pfeifroth, U., Träger-Chatterjee, C., Cremer, R., Trentmann, J., and Hollmann, R.: Surface Solar Radiation Data Set–Heliosat (SARAH)–Edition 1. Satellite Application Facility on Climate Monitoring, accessed 3 September 2016, doi:10.5676/EUM_SAF_CM/SARAH/V001, 2015.

Nie, J., Boos, W. R., and Kuang, Z. M.: Observational evaluation of a convective quasi-equilibrium view of monsoons, J. Climate, 23, 4416–4428, 2010.

Noda, A.T., Oouchi, K., Satoh, M., Tomita, H., Iga, S.-I., and Tsushima, Y.: Importance of the subgrid-scale turbulent moist process: cloud distribution in global cloud-resolving simulations, Atmos. Res., 96, 208-217, doi:10.1016/j.atmosres.2009.05.007, 2009.

Orr, A., Bechtold, P., Scinocca, J., Ern, M., and Janiskova, M.: Improved middle atmosphere climate and forecasts in the ECMWF model through a nonorographic gravity wave drag parameterization, J. Climate, 23, 5905–5926, 2010.

Peyrillé, P. , Lafore, J., and Boone, A.: The annual cycle of the West African monsoon in a two-dimensional model: mechanisms of the rain-band migration, Q. J. Roy. Meteor. Soc., 142, 1473-1489, doi:10.1002/qj.2750, 2016.

Poan, E.D., Gachon, P., Dueymes, G., Diaconescu, E., Laprise, R., and Seidou Sanda, I.: West African monsoon intraseasonal activity and its daily precipitation indices in regional climate models: diagnostics and challenges, Clim. Dyn., 47, 9-10, 3113–3140, https://doi.org/10.1007/s00382-016-3016-8, 2016.

Posselt, R., Mueller, R. W., Stöckli, R., and Trentmann, J.: Remote sensing of solar surface radiation for climate monitoring – the CM-SAF retrieval in international comparison, Remote Sens. Environ., 118, 186–198, doi:10.1016/j.rse.2011.11.016, 2012.

Raymond, D. J., and Herman, M. J.: Convective quasi-equilibrium reconsidered, J. Adv. Model. Earth Syst., 3, M08003, doi: 10.1029/2011MS000079, 2011.

Raschendorfer, M.: The new turbulence parameterization of LM, COSMO Newsletter, 1, 89-97, 2001.

Rodríguez-Fonseca, B., Mohino, E., Mechoso, C. R., Caminade, C., Biasutti, M., Gaetani, M., García-Serrano, J., Vizy, E. K., Cook, K., Xue, Y., Polo, I., Losada, T., Druyan, L., Fontaine, B., Bader, J., Doblas-Reyes, F. J., Goddard, L., Janicot, S., Arribas, A., Lau, W., Colman, A., Rowell, D. P., Kucharski, F., and Voldoire, A.: Variability and predictability of West African droughts, J. Climate, 28, 4034–4060, 2015.

Roehrig, R., Bouniol, D., Guichard, F., Hourdin, F., and Redelsperger, J.-L.: The present and future of the West African monsoon: A process-oriented assessment of CMIP5 simulations along the AMMA transect, J. Climate, 6, 6471–6505, DOI: 10.1175/JCLI-D-12-00505.1, 2013.

Schrage, J. M., Augustyn, S., and Fink, A. H.: Nocturnal stratiform cloudiness during the West African monsoon, Meteorol. Atmos. Phys., 95, 73–86, DOI 10.1007/s00703-006-0194-7, 2007.

Schrage, J.M. and Fink, A.H.: Nocturnal continental low-level stratus over tropical West Africa: Observations and possible mechanisms controlling its onset, Mon. Weather Rev., 140, 1794–1809, https://doi.org/10.1175/MWR-D-11-00172.1, 2012.

Schuster, R., Fink, A.H., and Knippertz, P.: Formation and maintenance of nocturnal low-level stratus over the southern West African monsoon region during AMMA 2006, J. Atmos. Sci., 70, 2337–2355, https://doi.org/10.1175/JAS-D-12-0241.1, 2013.

Seifert, A.: On the parameterization of evaporation of raindrops as simulated by a one-dimensional rainshaft model, J. Atmos. Sci., 65, 3608–3619, https://doi.org/10.1175/2008JAS2586.1, 2008.

Sultan, B. and Janicot, S.: Abrupt shift of the ITCZ over West Africa and intra-seasonal variability, Geophys. Res. Lett. 27: 3353-3356, 2000.

Taylor, C. M., Gounou, A., Guichard, F., Harris, P. P., Ellis, R. J., Couvreux, F., and De Kauwe, M., Frequency of Sahelian storm initiation enhanced over mesoscale soil-moisture patterns, Nat. Geosci., 4, 430–433, doi:10.1038/ngeo1173, 2011.

Thorncroft, C. D., Nguyan, H., Zhang, C. and Peyrillé, P.: Annual cycle of the West African monsoon: regional circulations and associated water vapour transport, Q. J. Roy. Meteor. Soc. 137, 129-147, 2011.

van der Linden, R., Fink, A. H., and Redl, R.: Satellite-based climatology of low-level continental clouds in southern West Africa during the summer monsoon season, J. Geophys. Res. Atmos., 120, 1186-1201, doi:10.1002/2014JD022614, 2015.

Vogel, P., Knippertz, P., Fink, A. H., Schlueter, A., and Gneiting, T.: Skill of global raw and postprocessed ensemble predictions of rainfall over northern tropical Africa, Weather Forecast., 33, 369–388, https://doi.org/10.1175/WAF-D-17-0127.1, 2018.

Young, D. F., Minnis, P., Doelling, D. R., Gibson, G. G., and Wong, T.: Temporal interpolation methods for the Clouds and Earth's Radiant Energy System (CERES) experiment, J. Appl. Meteorol.,37, 572-590, 1998.

Xue, Y., De Sales, F., Lau, W. K.-M., Boone, A., Feng, J., Dirmeyer, P., Guo, Z., Kim, K.-M., Kitoh, A., Kumar, A., Poccard-Leclercq, I., Mahowald, N., Moufouma-Okia, W., Pegion, P., Rowell, D. P., Schemm, J., Schubert, S. D., Sealy, A., Thiaw, W. M., Vintzileos, A., Williams, S. F., and Wu, M.-L. C.: Intercomparison and analyses of the climatology of the West African monsoon in the West African Monsoon Modeling and Evaluation project (WAMME) first model intercomparison experiment, Clim. Dyn., 35, 1, 3–27, https://doi.org/10.1007/s00382-010-0778-2, 2010.

Xue, Y., De Sales, F., Lau, W.KM., Boone, A., Kim. K.-M., Mechoso, C. R., Wang, G., Kucharski, F., Schiro, K., Hosaka, M., Li, S., Druyan, L. M., Seidou, I., Wassila, S., Zeng, T. N., Comer, R. E., Lim, Y.-K., Mahanama, S., Song, G., Gu, Y., Hagos, S. M., Chin, M., Schubert, S., Dirmeyer, P., Leung, L. R., Kalnay, E, Kitoh, A., Lu, C.-H., Mahowald, N. M., and Zhang, Z.: West African monsoon decadal variability and surface-related forcings: second West African Monsoon Modeling and Evaluation Project Experiment (WAMME II), Clim. Dyn., 47, 11, 3517–3545 , https://doi.org/10.1007/s00382-016-3224-2, 2016.

Zängl, G. , Reinert, D. , Rípodas, P., and Baldauf, M.: The ICON (ICOsahedral Non-hydrostatic) modelling framework of DWD and MPI-M: Description of the non-hydrostatic dynamical core, Q. J. Roy. Meteor. Soc., 141, 563-579, doi:10.1002/qj.2378, 2015.

Zheng, X. , Eltahir, E. A., and Emanuel, K. A.: A mechanism relating tropical Atlantic spring sea surface temperature and West African rainfall, Q. J. Roy. Meteor. Soc., 125, 1129-1163, doi:10.1002/qj.1999.49712555604, 1999.

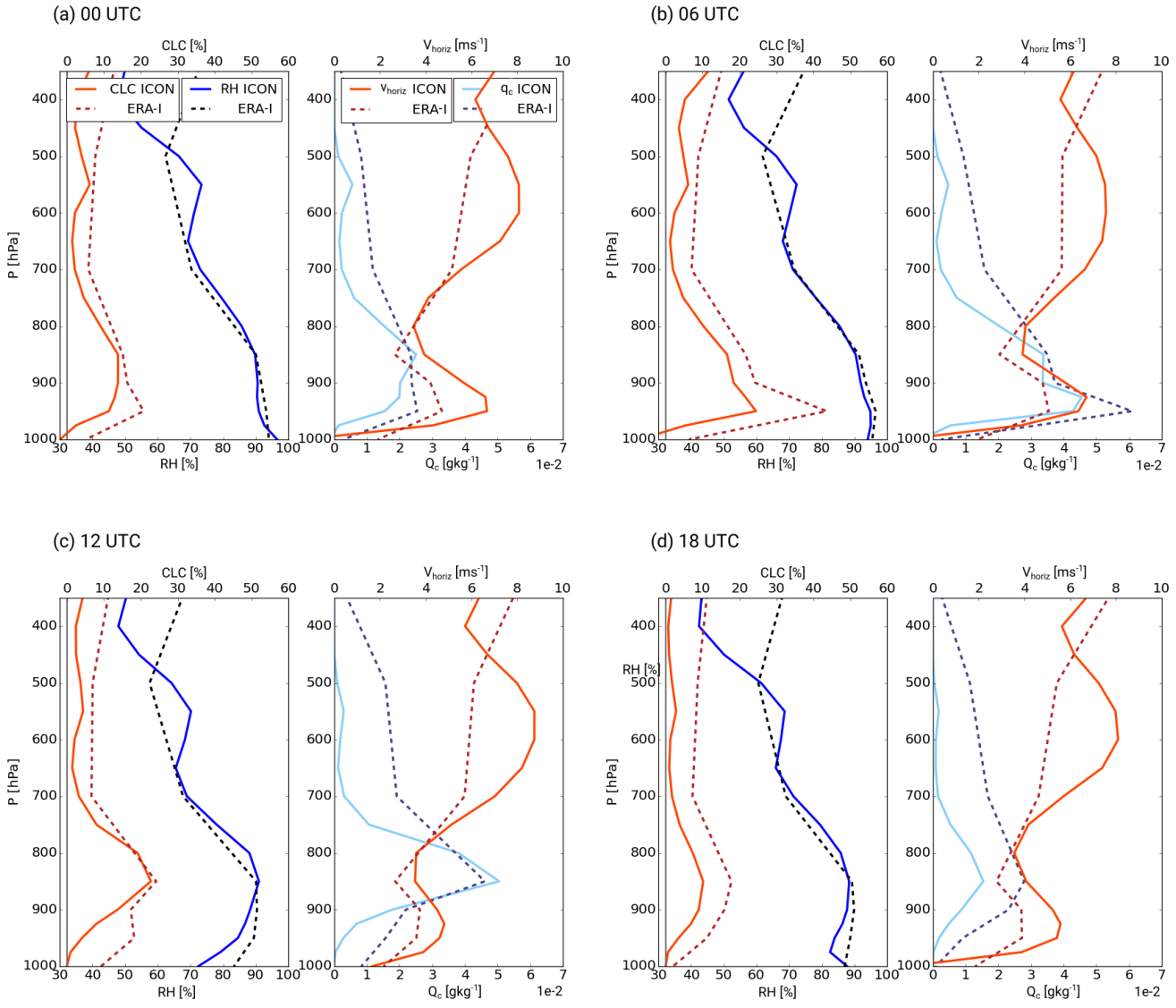

Figure S1. Average profiles of CLC and RH (left graph), v_{horiz} and components (middle graph) and q_c (right graph) for the monsoon season July - September. Averages over the DACCIWA area are shown as diurnal cycle where (a) is 00 UTC, (b) 06 UTC, (c) 12 UTC and (d) 18 UTC. Solid lines denote the ICON results with simulations started daily at 12 UTC and dashed lines denote the corresponding ERA-Interim fields.

S1 Supplementary Material

S1.1 Climatology and model evaluation

In addition to the general characterization of the meteorological conditions in southern West Africa for the variables precipitation and radiation, a brief discussion about the diurnal cycle of the vertical atmospheric structure is given for the wet monsoon

season July, August and September 2006. Comparison of ICON CLIM with ERA-I and observations confirms the applicability of the ICON model for the sensitivity experiments of the main article.

Figure S1 shows average profiles of cloud cover (CLC), relative humidity (RH), horizontal wind speed v_{horiz} as well as specific cloud water content q_c for 00, 06, 12 and 18 UTC (corresponding to local time in our study region). At 00 UTC the NLLJ is already well established and the low-level cloud deck is beginning to form (Fig. S1a). ICON shows a considerably stronger jet than ERA-I reaching 7 ms^{-1} at 925-950 hPa and consistently lower values in CLC, RH and q_c. In contrast to ERA-I, ICON tends to concentrate cloud water in the upper parts of the cloud deck around 850 hPa. The relatively small differences in RH between the two datasets (more than 90% from 830 hPa downwards) in contrast to differences in CLC and q_c illustrates a substantial sensitivity to the subgrid-scale cloud scheme or possibly differences in spatial variance of RH, as the dependance of CLC on RH is quadratic in ICON. The tendency of stronger NLLJ and less cloud was also found in many climate models (Hannak et al. 2017). At midlevels around 560 hPa ICON shows a secondary peak in v_{horiz}, CLC, RH and q_c not found in the overall smoother and moister ERA-I profiles.

At 06 UTC the NLLJ is very similar to 00 UTC but the low-level cloud deck increases markedly in cover and q_c accompanied by an increase in RH to values well above 95 % below 900 hPa (Fig. S1b). Maximum CLC occurs at 950 hPa reaching 25% in ICON and about 45% in ERA-I, which is more realistic (cf. van der Linden et al., 2015). Overall the discrepancies between the two models are qualitatively similar to 00 UTC (Fig. S1a). At midday (Fig. S1c), radiative heating lifts and dissolves the low-level cloud deck shifting the maximum in CLC and RH to 850 hPa, where a pronounced peak in q_c develops. Surface heating and turbulent mixing markedly slows down the low-level jet (e.g. 4.5 ms^{-1} in ICON) and decreases RH to under 90% below 900 hPa with ICON being substantially drier and less cloudy in that layer. Finally at 18 UTC (Fig. S1d) the low-level jet starts re-accelerating, keeping the generally higher values in ICON found at all times of day. The deep daytime mixing has reduced CLC and q_c and created an almost vertically constant offset between the two modeling systems. RH is already increasing at this time of day, particularly in ICON, where also the sharp gradient in v_{horiz} suggests a beginning decoupling of the surface. Such an early evening transition is consistent with observations as documented in Fig. 3d in Schuster et al. (2013). The comparison between the two datasets shows considerable biases at all times of day with generally higher low- and midlevel wind maxima in ICON but moister and more cloudy low levels in ERA-I. Investigating the reasons for these discrepancies is beyond the scope of this paper but the overall agreement in vertical structure and diurnal cycle suggests that sensitivities tested with ICON should be qualitatively meaningful.

S1.2 Temporal stability of opacitiy-induced effects

An additional aspect to be discussed is the response time of the atmospheric system to the imposed cloud modifications. To investigate this we use EXPL experiments, in which $f_{op} = 0.1$ is applied for the first 4 days but then switched off for 6 more days of simulation time. Control runs with $f_{op} = 1.0$ for all times were produced for comparison. As in EXPL, simulations were started every 4th day but run out to 10 days and two starting dates in August were added (3rd and 7th of August) to give better statistics for the time evolution. Figure S2 shows box-averaged 10-day time-series of RR, cover of low clouds CLC_{low} and that of high clouds CLC_{high} (below 800 hPa and above 400 hPa, respectively) for the DACCIWA region (Figs. S2a–c). The corresponding differences between the two sets of simulations are provided in the right-hand side panels of Fig. S2.

After the switch-off at 12 UTC on the fifth simulation day (i.e. after 96 hours), the differences in SSI and low-level T are reduced almost immediately (not shown), but for other variables the response is slower. RR shows the enhancement of afternoon and evening precipitation for $f_{op} = 0.1$ as in EXPL (Figs. S2a and f). The enhancement is still fully visible for the first 14 hours after switch-off, indicating that the influence of the forcing during the morning hours is already enough to generate more instability and trigger more convection later in the day. After that, differences between the two runs become negligible. Before the switch in f_{op}, CLC_{low} shows the familiar afternoon decrease and nighttime increase (Figs. S2b and g). On the day of the change, some signal remains until the morning of the following day, similar to RR. The small but on average slightly positive differences after that may be a reflection of increased surface fluxes after the strongly enhanced rainfall of the first five days. CLC_{high} (Figs. S2c and h) shows a considerably slower response. Differences between the two runs need one full diurnal cycle to establish and are then positive for the next three days. After the switch, there is a marked decrease

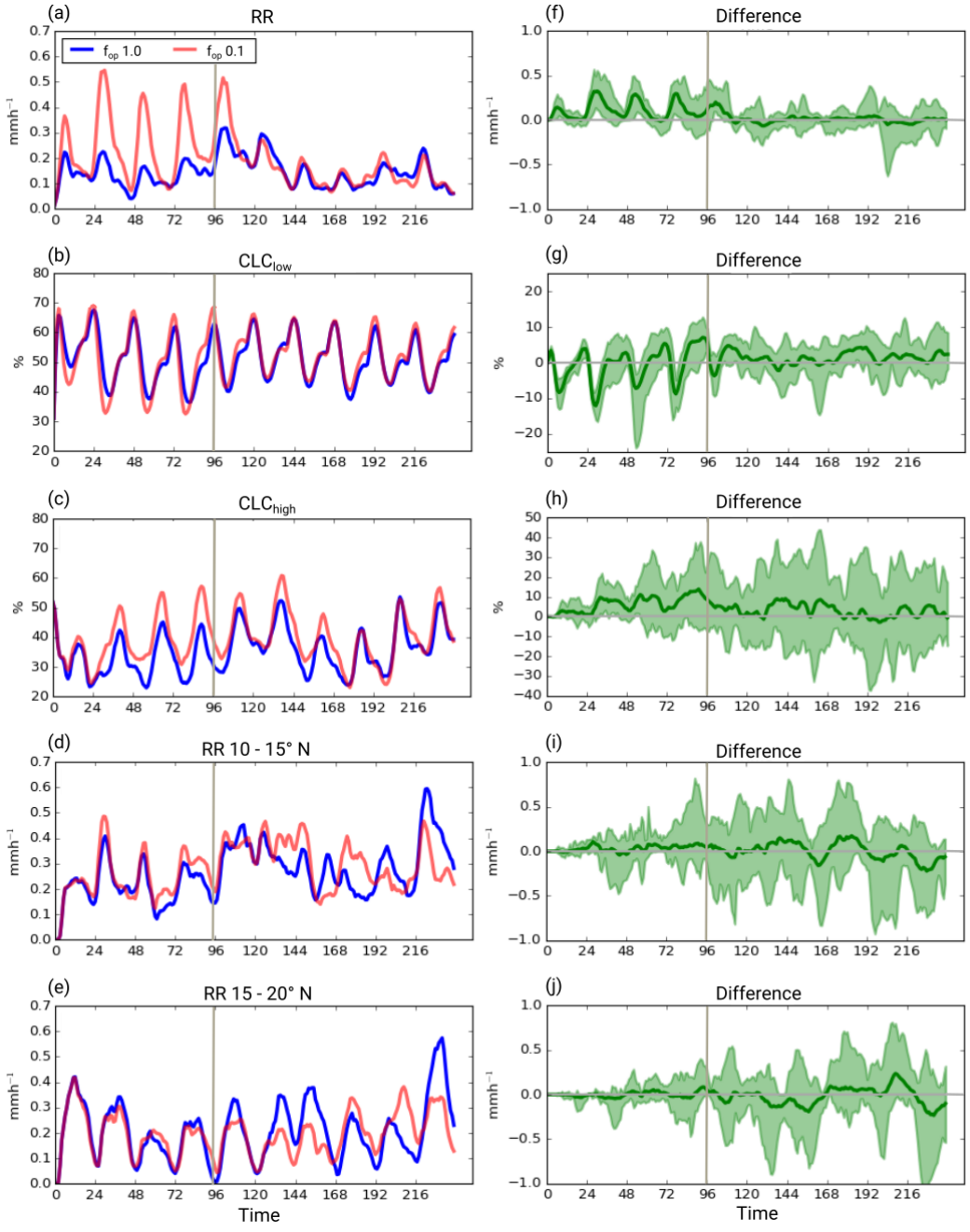

Figure S2. Time-series of RR (a), CLC_{low} (b) and CLC_{high} (c) of the experiments with $f_{op} = 1.0$ all the time (blue line) and f_{op} switched from 0.1 to 1.0 after 96 hours (orange line). Results are averaged over the DACCIWA box, for all 10 runs in July-August 2006. (d) and (e) depict similar averages of RR but for the northern boxes 15–20°N, 8°W–8°E and 15–20°N, 8°W–8°E, respectively. The corresponding differences are shown as green lines in (f)–(j), where the shaded area denotes the maximum and minimum values of the time-series. Switch-off time is indicated by a grey line in all panels.

in differences but then an overall tendency for relatively large values for two more days. This is consistent with Raymond et al. (2011), who show a considerably longer response time in the tropical upper troposphere than at low levels for a given perturbation.

Another interesting question is the impact on regions to the north, i.e. downstream of the DACCIWA box with respect to the monsoon flow. Figures S2d, e, i and j show corresponding plots for RR over the Sahelian regions 10–15°N and 15–20°N, both averaged over 8°W–8°E. For the former, again an initial response time of about one day is observed followed by a period of small positive differences. During the last five days of the simulation there is then no clear net difference between the two sets of experiments but much larger fluctuations. As these do not follow a strict diurnal cycle, we speculate that this is mostly a reflection of the overall chaotic nature of the atmosphere growing with leadtime. This conclusion is consistent with the similar behavior found for the 15–20°N band.

So in summary, this experiment shows that low-level variables such as SSI and T react almost immediately to changes in low cloud during the day. Low-level cloud cover and rainfall respond after one full diurnal cycle, while upper-level variables and neighboring regions show even longer responses, but also increasingly chaotic behavior. The latter is reflected in the growing shaded areas denoting the envelope of all runs in the bias in the right-hand side panels of Fig. S2.

S1.3 Table of acronyms

Table S1. Table of acronyms and abbreviations used in the main article.

Acronym	denotation
θ_e	equivalent potential temperature
CALIPSO	Cloud-Aerosol Lidar and Infrared Pathfinder Satellite Observation
CERES	Clouds and the Earth's Radiant Energy System
CM SAF	Satellite Application Facility on Climate Monitoring
CLC	cloud cover
CLC_{low}	low-cloud cover
CLC_{high}	high-cloud cover
CloudSat	satellite in A-train with cloud profiling radar
COSMO model	Consortium for Small-scale Modeling model
COSMO-EU	regional COSMO model for Europe
DACCIWA	Dynamics-Aerosol-Chemistry-Cloud Interactions in West Africa project
DWD	German weather service
EBAF-Surface	Energy Balanced And Filled surface irradiance
EBAF-TOA	Energy Balanced And Filled top of atmosphere irradiance
ECMWF	European Centre for Medium-Range Weather Forecasts
ERA-I	ERA Interim
EXPL	experiment with explicit convection
f_{op}	opacity factor
GERB	Geostationary Earth Radiation Budget
GPCP	Global Precipitation Climatology Project
GPCC	Global Precipitation Climatology Centre
ICON	Icosahedral Non-hydrostatic (numerical weather prediction model of DWD)
IFS	Integrated Forecasting System
ITD	Intertropical Discontinuity
MODIS	Moderate Resolution Imaging Spectroradiometer
MPI-M	Max Planck Institute for Meteorology
MVIRI	Meteosat Visible and Infrared Imager
NLLJ	nocturnal low-level jet
NPP	Suomi National Polar-orbiting Partnership
NWP	numerical weather prediction
OLR	outgoing longwave radiation

Acronym	denotation
OSR	outgoing shortwave radiation
p_{sfc}	surface pressure
PARAM	experiment with parameterised convection
PBL	planetary boundary layer
q_c	cloud liquid water content
q_i	cloud ice content
q_v	specific humidity
RH	relative humidity
RR	precipitation rate
RRTM	Rapid Radiation Transfer Model
SARAH	Surface Solar Radiation Data Set Heliosat
SEVIRI	Spinning Enhanced Visible and InfraRed Imager
SLEVE	smooth level vertical (coordinate)
SLI	surface longwave irradiance
SOCRATES	Suite Of Community RAdiative Transfer codes based on Edwards and Slingo
SSI	solar surface irradiance
SST	sea surface temperature
SWA	southern West Africa
SWITCH	experiment where opacity factor is switched to 1 after some time
T	temperature
TERRA	soil and vegetation model
TKE	turbulent kinetic energy
TMPA	TRMM Multisatellite Precipitation Analysis
TOA	top of atmosphere
TRMM	Tropical Rainfall Measuring Mission
v_{horiz}	horizontal wind speed
WAM	West African monsoon